Mannose supplements induce embryonic lethality and blindness in phosphomannose isomerase hypomorphic mice.

Vandana Sharma[1], Jonamani Nayak[1], Charles DeRossi[1a], Adriana Charbono[1], Mie Ichikawa[1], Bobby G Ng[1], Erika Grajales-Esquivel[2], Anand Srivastava[1b], Ling Wang[1], Ping He[1], David A Scott[1], Joseph Russell[1c], Emily Contreras[1d], Cherise M Guess[1e], Stan Krajewski[1], Katia Del Rio-Tsonis[2], Hudson H Freeze[1*]

1. *Sanford-Burnham Medical Research Institute (SBMRI), 10901 North Torrey Pines Road, La Jolla, CA 92037, USA.
2. Department of Biology, Miami University, 700 East High Street, Oxford, OH 45056, USA.

*Corresponding author

Present Address:

a Center for Child and Adolescent Medicine and Center for Metabolic Diseases Heidelberg, Department Kinderheilkunde I, Heidelberg, Germany.

b Global Institute of Stem Cell Therapy and Research, 4370 La Jolla Village Drive, San Diego, CA92122, USA.

c Janssen Research & Development, LLC, 3210 Merryfield Row, San Diego, CA 92121, USA.

d Riley Children's Specialists, 11725 N. Illinois Street, Suite 240, Carmel, IN 46032, USA.

e St. Jude Children's Research Hospital, 262 Danny Thomas Place, Memphis, TN 38105-2794.

Short title for running foot: Phosphomannose isomerase hypomorphic mice

Abbreviations:

CDG, Congenital Disorders of Glycosylation; MPI or *MPI* or *Mpi*, phosphomannose isomerase; HK, hexokinase; PMM2, phosphomannomutase; Man-6-P, mannose-6-phosphate; Glc-6-P, glucose-6-phosphate; Fru-6-P, fructose-6-phosphate; DMEM, Dulbecco's modified Eagle's medium; TNFα,tumor necrosis factor-alpha; PLE, protein losing enteropathy; AAT, alpha-1 antitrypsin; BSTFA, *N*,*O*-bis[trimethylsilyl]trifluoroacetamide; mouse embryonic fibroblasts, mEFs; TCA, trichloroacetic acid; WT, wild-type; h, hour; min, minutes; s, seconds; PGI, phosphoglucose isomerase; G6PD, glucose-6-phosphate dehydrogenase; PBS, phosphate buffered saline; BSA, bovine serum albumin; GC-MS, Gas Chromatography-Mass Spectrometry; FACE, Fluorophore-Assisted Carbohydrate Electrophoresis*;* *AGA*, aspartyl glucosaminidase;β-hex, β-hexosaminidase.

Abstract

Patients with congenital disorder of glycosylation (CDG), type Ib (MPI-CDG or CDG-Ib) have mutations in phosphomannose isomerase (*MPI*) that impair glycosylation and lead to stunted growth, liver dysfunction, coagulopathy, hypoglycemia and intestinal abnormalities. Mannose supplements correct hypoglycosylation and most symptoms by providing mannose-6-P (Man-6-P) via hexokinase. We generated viable *Mpi* hypomorphic mice with residual enzymatic activity comparable to that of patients, but surprisingly, these mice appeared completely normal except for modest (~15%) embryonic lethality. To overcome this lethality, pregnant dams were provided 1-2% mannose in their drinking water. However, mannose further reduced litter size and survival-to-weaning by 40% and 66%, respectively. Moreover, ~50% survivors developed eye defects beginning around mid-gestation. Mannose started at birth also led to eye defects but had no effect when started after eye development was complete. Man-6-P and related metabolites accumulated in the affected adult eye and in developing embryos and placentae. Our results demonstrate that disturbing mannose metabolic flux in mice, especially during embryonic development induces a highly specific, unanticipated pathologic state. It is unknown whether mannose is harmful to human fetuses during gestation however, mothers at-risk for having MPI-CDG children who consume mannose during pregnancy hoping to benefit an affected fetus *in utero* should be cautious.

Keywords:

Mannose-6-phosphate, Congenital Disorder of glycosylation, MPI-CDG, lens, eye-defects

Introduction

A potentially lethal form of rare congenital disorder of glycosylation (CDG), Type Ib (CDG-Ib, or MPI-CDG) can be treated with mannose as a dietary supplement (1). Supplementation overcomes impaired glycosylation caused by hypomorphic mutations in *MPI* because mannose bypasses the impaired conversion of fructose-6-P (Fru-6-P) to Man-6-P, which is the major source of Man-6-P derived from glucose. Mannose alleviates patients' stunted growth, hypoglycemia, liver dysfunction, coagulopathy, and protein-losing enteropathy (2). Exogenous mannose is converted to Man-6-P by hexokinase (HK), replenishing this deficient precursor needed for multiple glycosylation pathways including the N-glycosylation pathway via phosphomannomutase (PMM2); excess Man-6-P is catabolized by the residual MPI activity (Scheme1). Patients on this therapy survive and lead a normal life without any obvious side effects (2).

To model MPI-CDG and follow the effects of mannose therapy, we previously knocked out the single *Mpi* gene in mice, leading to death at E11.5 due to abnormalities in both placenta and the embryo. Mannose could not rescue because Man-6-P accumulates to toxic levels limiting ATP and inhibiting several glycolytic enzymes (3). However, because MPI-CDG patients have residual enzymatic activity, hypomorphic mice would offer a more patient-relevant model than would a complete *Mpi*-knockout. Here, we describe a viable, hypomorphic mouse line containing a patient-derived mutation that reduced enzymatic activity and altered mannose metabolism, as predicted. While a minority of mutant embryos died *in utero,* surprisingly, adolescent and adult mice had none of the expected symptoms reported in MPI-CDG patients; these *Mpi*-deficient mice had a "sub-clinical phenotype". However, if dams consumed mannose during pregnancy, most of the *Mpi* hypomorphic embryos died and nearly half of the survivors were born with severe ocular defects. The combination of reduced enzymatic activity and the increased mannose load altered its metabolic flux leading to Man-6-P accumulation in the eyes.

Mannose is widely used as a "natural" treatment for urinary tract infections, this seemingly innocuous sugar may have a negative impact for some pregnant women. While the frequency of MPI-CDG is unknown, women at-risk for having subsequent MPI-CDG children who intend to take mannose as a "prenatal therapy" may inadvertently cause other side effects.

Materials and Methods

Materials - Most of the reagents were purchased from Sigma-Aldrich, St. Louis, MO, USA. Dulbecco's modified Eagle's medium (DMEM) with 1g/L glucose was purchased from Corning Cellgro, Manassas, VA,

USA. Fetal bovine serum (FBS) was obtained from Hyclone Laboratories, Logan, UT, USA. [2-^{3}H]-Mannose was procured from Perkin Elmer, Boston, MA, USA. Protease inhibitor cocktail was purchased from Roche Diagnostics, Indianapolis, IN, USA. Carrier-free recombinant human tumor necrosis factor-alpha (TNFα) and recombinant mouse alpha-1 antitrypsin (AAT) were purchased from Cell Sciences, Canton, MA, USA and ICL Inc., Portland, OR, USA respectively. *N*,*O*-bis[trimethylsilyl]trifluoroacetamide (BSTFA) was procured from Thermo Scientific, Pennsylvania. Z-fix and Bouin's solution for tissue fixation were obtained from Anatech Ltd, Battle Creek, MI, USA and Ricca Chemical, Arlington, TX, USA respectively. Protein was measured by using the Pierce BCA protein estimation kit from Thermo Scientific, Waltham, MA, USA.

Primers and probes: Primers were synthesized by Integrated DNA Technologies, San Diego, CA, USA. The following sequences were used:

(a) Primers:

M14a-F1 (GTAGGCCAGTGGACTAATGAAGCG),

FnFL-F3 (ATGGCCGCTTTTCTGGATTCA),

LoxP-R1 (CCTCAGCCCAAGCACCCAAATA),

LoxP-F1 (CCTTAGCTCCTTGCCCGA-CTGG),

(b) Probes for Southern blot:

5'probe -P717_01(GCAGGTGCCTGTGGAGGTCAG) and
P717_02 (CTTGTTAGGGGTGCCTGGATAGA,

3' probe – P717_03 (GTGCGGCCATGTCCC TAACT) and
P717_04 (GATGTCCCCTGAACTGATTGTCTT).

Antibodies: Antibodies used in this study include antisera against alpha antitrypsin (AAT) from Siemens, Marburg, Germany, chicken anti-mouse AAT IgY from ICL Inc., Portland, OR, USA and alkaline phosphatase-conjugated goat anti-chicken IgY IgG from Jackson ImmunoResearch, West Grove, PA, USA. The MPI specific antibody was raised in our laboratory and has been described previously (4). The AP-2 antibody was obtained from the Developmental Studies Hybridoma Bank and was developed under the auspices of the National Institute of Child Health and Human Development and maintained by The University of Iowa, Department of Biological Sciences, Iowa City, IA 52242, USA. Antibodies against Brn3a, S-opsin and M/L-opsin were purchased from Chemicon International, Inc., Temecula, CA, USA. The anti-Pax6 antibody was purchased from Santa Cruz Biotechnology, Dallas, TX. The secondary antibodies were purchased from Molecular Probes, Inc. Eugene, OR, USA.

Animals: SBMRI's Institutional Animal Care and Use Committee approved all the animal studies. *Mpi*$^{Y255C/Y255C}$ (KI/KI) mice were created in C57BL/6 strain. *Mpi*$^{+/+}$(WT) animals obtained from heterozygous, *Mpi*$^{Y255c/+}$(Het) crosses were used as controls. KI/KI animals were then crossed with mice heterozygous for the *Mpi* knockout allele (M*pi*$^{+/-}$) on a mixed background (C57BL/6 and 129/SvEV) to create *Mpi*$^{Y255C/-}$ (KI/KO) mice. All the mice were maintained on a 12h dark/12h light cycle.

Genotyping of mice: Genomic DNA was extracted from tail clips and PCR was performed to confirm the genotype using primers M14a-F1 and LoxP-R1. Hotstart Taq Blue Mastermix^{TM} (Denville Scientific Inc., Metuchen, NJ, USA) was used for the amplification with the following cycle conditions: 94^{o}C for 15 min for hotstart, 30 cycles – 94^{o}C for 30 s, 60^{o}C for 30 s and 72^{o}C for 1.5 min and 72^{o}C for 5 min at the end of 30 cycles. On 2% agarose gel, WT showed 650 bp band and KI/KI, 750 bp band and heterozygous mice showed both the bands (Supplementary figure. 1c).

Isolation of murine embryonic fibroblasts isolation: Mouse embryonic fibroblasts (mEFs) were isolated from KI/KI embryos at E11.5 as previously described (3). No additional mannose was required to propagate these mEFs.

^{3}H-Mannose injection in the mice: 50 µCi [2-^{3}H]-Mannose was injected in the tail vein of three mice per group (WT, KI/KI and KI/KO). Blood (20-30 µl) was collected at 5, 15, 30, 60, 90, 120 and 180 min, diluted with phosphate buffered saline (PBS) and centrifuged at 1000 rpm. Diluted plasma was used to estimate the amount of $^{3}H_2O$, [2-^{3}H]-Mannose and trichloroacetic acid (TCA) precipitable labeled glycoproteins. After 3 h, the mice were humanely sacrificed and their organs were collected to determine [2-^{3}H]-Mannose in the tissue glycoproteins.

Analysis of $^{3}H_2O$ in the plasma*: A* 10 µl aliquot of plasma was used to determine radioactivity with and without evaporation to dryness. The difference was defined as the amount of $^{3}H_2O$ in 10 µl of blood (5).

Analysis of [2-^{3}H]-Mannose in the plasma*:* Free [2-^{3}H]-Mannose in the plasma was determined by using hexokinase and recombinant human MPI to convert it to $^{3}H_2O$, before evaporating it. The difference between the radioactivity level before and after evaporation was defined as the amount of [2-^{3}H]-Mannose in plasma (5).

Precipitation of plasma proteins: 20 µl plasma was diluted to 200 µl with PBS and an equal volume of 20% trichloroacetic acid (TCA) was added. The samples were incubated on ice for an hour and centrifuged at 14,000

g for 15 min. The protein pellet was washed once with acetone and re-suspended in 0.2 N sodium hydroxide. The amount of ^{3}H-radiolabel in the precipitated protein was determined.

Stable Isotope Label: The cells were labeled with stable isotopes [1,2-^{13}C]-Glucose and [4-^{13}C]-Mannose and isolated glycans were analyzed by gas-chromatography-mass spectroscopy (GC-MS) as described before (6).

Enzymatic activity assays: A small section of each organ to be tested was minced and disrupted by sonication in chilled 50 mM HEPES buffer (pH 7.4) containing protease inhibitors. Tissue lysate was centrifuged at 14,000 g for 10 min at 4^{o}C. The supernatant was collected, and the amount of protein was measured by using the Pierce BCA protein estimation kit. A 15 µg aliquot of protein was used to estimate MPI activity. A standard coupled assay using phosphoglucose isomerase (PGI) and glucose-6-phosphate dehydrogenase (G6PD) with NADPH readout at 340 nm was used to estimate MPI activity in the organ lysate (7). The original protocol was modified to a final volume of 210 µl and enzyme activity was measured in a 96 well plate for 2 h using a microplate reader (SpectraMax Plus^{384} Molecular Devices, California, USA).

Western blot analysis: A total of 50 µg of organ lysate (as described above) was separated by 12% SDS-PAGE and transferred to a nitrocellulose membrane. Unbound sites were blocked overnight at 4^{o}C with PBS containing 5% bovine serum albumin (BSA). The membrane was probed with primary anti-mouse MPI diluted in PBS/2%BSA for 1 h at room temperature followed by three 10 min washes and then probed with horseradish peroxidase (HRP)-conjugated anti-rabbit secondary antibody at 1:2000 dilution in PBS/2%BSA for 1 h at room temperature. After three washes, the blot was developed by using BCIP substrate for HRP.

Blood/Serum Analysis: Glucose levels were determined by using FreeStyle glucometer and glucose strips from Abbot, Alameda, CA, USA. Several comprehensive parameters of freshly drawn blood were measured by using VetScan VS2 instrument (Abaxis, Union city, CA, USA). Hematocrit analysis was done by using a VetScan HM2 analyzer (Abaxis, Union city, CA, USA).

Fecal AAT estimation: Fecal extracts were prepared as described previously (8) and AAT was measured by non-competitive ELISA. Briefly, 96-well plates were coated with 100 µl of diluted antisera against human AAT, blocked with 1% BSA, washed with PBS and incubated with 100 µl of fecal extract (diluted 1:50 with PBS) or standards; all steps were performed for 1 h at 37^{o}C. Wells were washed with PBS and incubated with 100 µl of 0.4 µg/ml primary chicken anti-mouse AAT IgY prepared in 1%BSA, 0.05% Tween 20 for 18-24 h at 4^{o}C. After washes with 0.05% Tween in PBS, incubated with 100 µl of 0.25 µg/ml alkaline phosphatase-

conjugated goat anti-chicken IgY prepared in 1% BSA, 0.05% Tween 20 for 2 h at 37^{o}C. This was followed by washes and color development using 4-nitrophenyl phosphate as substrate. Absorbance was measured at 405 nm using microplate reader (SpectraMax Plus^{384}, Molecular Devices, Sunnyvale, CA). The amount of fecal AAT (ng/ml, feces extract) was derived from standard curve and reported as mean μg AAT per gram of dried stool.

Serum mannose determination by Gas Chromatography-Mass Spectrometry (GC-MS): Mannose was estimated by using a previously described method (9). Briefly, 10 μl serum and mannose standards were derivatized by adding of 50 μl hydroxylamine hydrochloride (50 mg/ml) in 1-methyl imidazole and incubation at 65^{o}C for 30 min. Then 100 μl acetic anhydride was added. Extraction was done with 100 μl chloroform and 200 μl water. After vortexing and centrifuging the samples, the aqueous layer was removed and re-extracted once more with water. The chloroform layer containing sugars was dried and solubilized in chloroform for GC-MS analysis (GCMS-QP2010 Plus, Shimadzu, Japan).

In vivo imaging of embryos in utero: Timed matings were set up for WT and KI/KI mice supplemented with 5% mannose in their drinking water. Females were checked for the presence of a vaginal plug the following morning to confirm the mating. The Vevo 770 (VisualSonics, Toronto, Canada), *in vivo* micro-imaging system was used with the RMV scan-heads 708 and 703 at a center frequency of 55 MHz and 35 MHz respectively to visualize embryos in pregnant mice starting at E6.5.

Histological examination of the tissues: Freshly dissected tissues or embryos were immediately fixed in buffered zinc-formalin, Z-fix. Bouin's solution was used to fix the entire head with eyes after birth. Paraffin embedded sections (5 microns thick) were cut and then stained with hematoxylin and eiosin (H&E) for structural analysis using the Aperio's scanscope slide scanning system (Aperio Technologies Inc, Vista, CA). Morphometric measurements were performed with Aperio Scanscope software, Imagescope.

Immunohistochemistry: The sections were de-paraffinized and antigen retrieval was performed in 0.01M sodium citrate for 30 min. Permeabilization was done with 1% saponin. The sections were blocked with 10% normal goat serum (for Brn3a, S-opsin and M/L-opsin) or 10% donkey serum (for Pax6 and AP-2), and incubated overnight at 4°C with the following diluted primary antibodies – Brn3a (1:10), S-opsin and M/L-opsin (1:200), Pax6 (1:100) and AP-2 (1:10). Next, fluorescently tagged secondary antibody was added. After thorough washing, Vectashield (Vector Laboratories, Burlingame, CA) was added and sections were sealed with a coverslip. Confocal images (size 1024 × 1024) were obtained sequentially on a Zeiss 710 Laser Scanning

Confocal System (Germany) using either a 20x/0.80 NA WD=0.55 objective lens or EC Plan-Neofluor 40x/0.75 M27 objective lens. Results were confirmed using three different biological samples. Quantification consisted of using Image J software to count the number of immunopositive cells in two different confocal images (1024 x 1024 taken at 40X) of the posterior region of three different eyes.

Mannose-6-phosphate Assay*:* The embryo, placenta and eye extracts were prepared as previously published (10). The method for Man-6-P estimation was modified from a protocol originally designed for glucose-6-phosphate estimation (11). We used a coupled enzyme assay, which uses phosphomannose isomerase (MPI), phosphoglucose isomerase (PGI) and glucose-6-phosphate dehydrogenase (G6PD) to convert Man-6-P to glucose-6-phosphate (Glc-6-P) with a final fluorescence readout. This method was optimized and validated by estimating Man-6-P in the mixtures containing known amounts of Man-6-P, Fru-6-P and Glc-6-P or adding known amounts of Man-6-P to tissue lysates. The values obtained by this method were comparable to the results obtained by using Fluorophore-Assisted Carbohydrate Electrophoresis (FACE) (12, 13). Briefly, 20 µl tissue extract of each sample type was dispensed in different wells of a black assay plate. Depending on the number of samples, two sets of reaction mix were prepared containing 50 mM HEPES, 1mM magnesium chloride, 100 µM NADP, 10 µM resazurin and 0.25 units diaphorase in a total volume of 80 µl per sample. MPI, PGI and G6PD (0.25 units/sample) were added to one set (F3) and only G6PD and PGI (0.25 units/sample) were added to the other set (F2). Another mix (Fb) containing G6PD, but devoid of NADP, was prepared to determine the background due to the endogenous NADP in each sample. An 80 µl aliquot of the mix was added to the wells containing 20 µl of the extract. After 15 min, fluorescence was recorded at excitation wavelength 530 nm and emission at 590 nm using Flexstation III (Molecular Devices, Sunnyvale, CA, USA). Background fluorescence (Fb) was subtracted from all the samples (F3 and F2). Difference between the fluorescence values (F3-F2) was used to calculate picomols (pmols) of Man-6-P using a standard curve generated with known amounts of Glc-6-P in 20 µl deionized water and 80 µl reaction mix containing G6PD.

GC-MS analysis of metabolites in the eyes – The eyes were crushed and washed once with cold PBS. Then, 100 µl chilled 0.1 M acetic acid with 3 nmol arabitol (internal standard) was added to the tissue and the mixture was sonicated briefly on ice. The samples were centrifuged at 8000 g for 5 min in a cold centrifuge and the supernatant was collected. Extraction was repeated one more time and the supernatants were combined. The extract was lyophilized, derivatized with hydroxylamine hydrochloride and *N,O*-bis[trimethylsilyl]trifluoroacetamide (BSTFA) and subjected to GC-MS (GCMS-QP2010 Plus, Shimadzu, Japan) according to a method as modified from Halket *et al* (14).

Vision test: Optokinetics was measured by using an optometer with motorized drum painted with black and white strips, which was built in-house at The Scripps Research Institute. The measurements were done under photopic conditions with light intensity of 150 lux. The mouse was placed on the wire mesh inside the drum and allowed to acclimate for 5 min without rotation and then for 30 s with rotation. The drum rotation (2 rotations/min) went clockwise for 1 min and then continued anti-clockwise direction for 1 minute with an interval of 30 s between the rotations. The animals with normal vision followed the movement of the rotating drum where as the ones with impaired vision failed to track the drum rotations. Visual response was measured by recording the number of head turns during drum rotations.

Results

Selection of MPI mutation: Since MPI-CDG patients have 3-20% residual MPI activity (1), we wanted to make a hypomorphic mouse line with similar residual activity to model the disorder and test mannose therapy. To identify a candidate, eight mutations from patients with confirmed MPI-CDG were introduced into the mouse *Mpi* gene to obtain the following amino acid changes: S102L, D131N, M138T, R152Q, R219Q, Y255C, I398T, R418H. Subsequently, mutant MPI constructs were expressed in mpi-null yeast strain SEY6210delpmi40::URA3 and activity was determined (Table 1). Mutation Y255C (TAC→TGC) retained ~12% activity (Table.1), which was confirmed by expression in CHO, COS7 and $Mpi^{-/-}$mEFs and consistently had 8-14% activity (data not shown). Y255C was selected to generate a knock-in mouse line as described in the supplement and supplementary Fig.1.

Hypomorphic mice have modest embryonic lethality: Both $Mpi^{Y255C/Y255C}$ (KI/KI) and $Mpi^{Y255C/-}$ (KI/KO) mice were viable. Heterozygous crosses (KI/+ x KI/+) showed a small, but significant (p=0.004) decrease of 16% below the expected number of KI/KI animals indicating modest embryonic lethality (Table 2). Similarly, homozygous (KI/KI x KI/KI) crosses produced litters that were significantly (p = 0.01) smaller than WT animals [WT – 8.6 (n=46) vs KI/KI – 7.5 (n=33)]. KI/KI survivors had normal weight gain (Supplement fig.2) and life span, showing no visible abnormalities in the organs as monitored by dissections at different times up to 13 months (data not shown).

Hypomorphic mice have reduced MPI activity and protein in various organs: KI/KI mice were predicted to have ~8-14% residual MPI activity and KI/KO mice ~4-7% activity compared to WT. Table 3 shows the result of enzymatic assays of different organ lysates. In KI/KI mice, the enzyme activity was reduced to approximately 18% in heart and nearly 2-3% in small intestine and liver (Fig.1a). KI/KO small intestine and

liver had 4- and 6-fold lower MPI activity, respectively than those of KI/KI (Fig.1a). Assays of mixed extracts of different organs showed no evidence for the presence of inhibitors or activators. In spite of these unexpected low activities in liver and small intestine, all mutant animals appeared to be healthy and none had any abnormal hepato-intestinal pathologic features on histochemical analysis (data not shown). Residual MPI protein antigen ranged from 25%-45% in various tissues from KI/KI mice and 14%-33% in KI/KO mice (Fig.1b). Our results clearly demonstrate reduced MPI protein and enzyme activity in hypomorphic mice, similar to that in fibroblasts and leukocytes of MPI-CDG patients (1).

Reduced MPI alters mannose flux in hypomorphic mice: Reduced MPI activity is predicted to increase mannose flux towards glycoprotein synthesis and decrease its catabolism (6). To confirm this, we labeled mice, organ cultures and mouse embryonic fibroblasts (mEFs) with [2-^{3}H]-Mannose and measured label incorporation into glycoproteins and catabolic production of $^{3}H_2O$ ([2-^{3}H]-Mannose $\rightarrow$ [2-^{3}H]-Man-6-P $\rightarrow$ Fru-6-P + $^{3}H_2O$). Reduced MPI should increase label incorporation into proteins and decrease catabolism of [2-^{3}H]-Mannose to $^{3}H_2O$ (Scheme 1). As seen in Fig.2a, KI/KI mEFs incorporated 5-fold more [2-^{3}H]-Mannose into glycoproteins than did WT, similar to the phenomena seen in the fibroblasts of patient with MPI-CDG (Fig.2b). Compared to WT mice, KI/KI and KI/KO mice injected with 50μCi [2-^{3}H]-Mannose in the tail vein had a reduced rate of production of $^{3}H_2O$ in serum (Fig.2c) together with a 5- to 6- fold increase in [2-^{3}H]-Mannose incorporation in serum glycoproteins (Fig.2d). Labeling of organ explants *ex vivo* showed 2- to 6- fold higher incorporation of [2-^{3}H]-Mannose in glycoproteins from KI/KI organs (Fig.2e), levels similar to those of mEFs and MPI-CDG patient fibroblasts (Fig.2a and b). We also labeled mEFs from WT and KI/KI mice with the stable isotopes – [1,2-^{13}C]-glucose and [4-^{13}C]-mannose under physiological conditions of 5 mM glucose and 50 μM mannose. Mannose directly contributed approximately 25% of mannose to WT N-glycans. This contribution increases by 2.3-fold to 57% in KI/KI mEFs with reduced MPI activity (data not shown). These results show that *Mpi* hypomorphic mice clearly have altered mannose metabolic flux due to the decreased activity.

Since the biochemical difference between KI/KI and KI/KO mice was small, only KI/KI mice on the pure C57BL/6 background were used in subsequent experiments.

KI/KI mice do not mimic MPI-CDG symptoms despite altered mannose metabolism: The patients with MPI-CDG are often hypoglycemic and have elevated serum alanine transaminase (ALT) and aspartate aminotransferase (AST) indicating liver pathology. They also have hypoalbuminemia and low antithrombin III (ATIII) levels, liver fibrosis, and some have intestinal villus atrophy and protein losing enteropathy (PLE).

We comprehensively analyzed serum from WT and KI/KI mice aged 3 and 10 months. No major differences existed in serum parameters of WT and KI/KI mice at any age (data not shown). KI/KI mice have normal glucose and liver enzymes. Potassium, an indicator of renal function, was significantly ($p = 0.01$) higher in KI/KI animals (7.5 mmol/L) than in WT (7.05 mmol/L), but was still within the normal range for mice. KI/KI mice had normal kidney function with no evidence of either proteinuria or increased blood urea nitrogen (BUN) concentration. The results of hematocrit analysis did not show any difference in the numbers of various blood cells except for slight but significant ($p = 0.02$) decrease in RBCs of KI/KI mice ($10.8 \pm 0.2 \times 10^{12}$/l) from that in WT mice ($11.06 \pm 0.1 \times 10^{12}$/l). However, this decreased amount was within the normal range for mice. Lysosomal enzymes, aspartyl glucosaminidase (AGA) and β-hexosaminidase (β-hex) are elevated in CDG-I patients (15), but in *Mpi* hypomorphic mice these activities (AGA – 9.7 ± 0.77 nmols/hr/ml, β-hex – 33.4 ± 4.5 nmols/min/ml) were no different from WT (AGA – 10.5 ± 0.73 nmols/hr/ml, β-hex – 36.2 ± 8.3 nmols/min/ml). Plasma proteins such as transferrin and alpha 1 antitrypsin (AAT) and coagulation factors such as antithrombin III, and factor XI are affected in MPI-CDG patients (16) but they were unaltered in KI/KI mice based on western blots (data not shown). Histological analysis of various organs, including liver and intestine at 3, 5, 7 and 13 months showed no morphological changes (data not shown) confirming that no visible pathology was present even in older mice. Because some patients with MPI-CDG have PLE (ie. loss of plasma proteins through small intestines), we also determined enteric protein loss in WT and KI/KI mice by measuring fecal AAT. KI/KI mice had neither enhanced levels of fecal AAT at basal state nor increased susceptibility to enteric protein loss when systemically challenged with TNFα, which is known to increase intestinal permeability (17) (Supplementary Fig.3). Our observations demonstrate that, despite having altered mannose metabolism and reduced MPI activity levels similar to those of patients with MPI-CDG, KI/KI mice failed to mimic any of the expected MPI-CDG symptoms.

Effects of mannose supplements:

There was a small but significant reduction in the number of KI/KI pups from heterozygous breeding (Table 2). We assumed that this was due to impaired glycosylation during embryogenesis and that the lethality would be rescued by providing mannose to the dams in their drinking water. Providing mice with 1% (w/v) mannose in their drinking water (60-80 mg/100 g body weight per day) is equivalent to the therapeutic doses given to patients with MPI-CDG (80-100 mg/100 g body weight per day). We supplied 0, 1, 2 and 5% mannose in the drinking water of WT and KI/KI dams and also to 6-8 week old mice.

Supplementing 1 – 5 % mannose in the drinking water of 6-8 week old hypomorphic mice had no obvious ill effects for over 4-6 months. They were healthy and grew normally confirming no toxic effects of mannose

therapy, which is also consistent with results in human studies. However, providing mannose to dams was lethal to the developing embryos. Crossing heterozygous KI/+ mice did not produce any KI/KI progeny when dams drank water containing 5% mannose (Table 4). Crossing homozygous KI/KI mice gave the same results. Ultrasound analysis of the dams showed that implantation occurred, but embryos were resorbed over time (Fig.3). Dissections at E13.5 revealed normal development of WT embryos (Fig.4a,b) and abnormal hemorrhaged placenta and resorbed embryos for KI/KI (Fig.4c).The results of histology analysis also showed a grossly disorganized placenta with a labyrinth layer (La) devoid of blood vessels and embryonic erythrocytes, abnormally organized giant cells (GC) and an expanded spongiotrophoblast (Fig.4.d,e).

KI/KI dams supplemented with 1% and 2% mannose produced live offspring, but litter size was significantly smaller than that of WT controls. Extensive placental hemorrhage occurred in the 5% mannose-supplemented group but not in the 2% mannose-fed KI/KI dams. However, placental size was significantly smaller than WT at various embryonic stages (Fig.5a). Sectioning of intact uteri bearing embryos (E8.5) showed developmental delay and abnormalities in KI/KI embryos that were not present in age-matched WT embryos (Fig.5b,c). These affected embryos would eventually die before birth.

The results here clearly show adverse effects of mannose supplementation on both placentae and embryos. Dams continued nursing on 1 or 2% mannose during weaning, but pup survival showed a dramatic dose-dependent decrease vs. controls (Table 5). The causes of death could not be investigated because most pups were reported as missing (most likely, cannibalized by the mother).

***Man-6-P accumulates in KI/KI embryos and placentas from dams drinking mannose-supplemented water*:** KI/KI mice given 1% and 2% mannose supplements significantly increase plasma mannose by 1.3 – 1.5 fold compared to mannose levels of those given plain water (Fig.6). WT mice also showed a 50% increase in mannose levels with 2% mannose, which is consistent with the results of earlier studies (18, 19).

At E11.5, MPI specific activities in placental and whole embryo lysates of KI/KI mice were 6%-7% of those in WT (Table 3). None of the organs from WT or KI/KI adult mice supplemented with mannose showed significant Man-6-P accumulation (data not shown). In contrast, baseline Man-6-P was higher in both KI/KI placenta and embryos compared to that in WT. There was an additional increase by ~2.5 fold upon 1%-2% mannose supplementation (Fig.7a, b). Man-6-P content in the embryos of WT dams supplemented with 2% mannose was comparable to that of KI/KI mice without mannose and neither group show any ill effects. Our previous studies on *Mpi*-null mice show that increased Man-6-P can cause ATP depletion and death (3).

However, ATP levels of E11.5 embryos and placentae from mannose-supplemented KI/KI and WT dams were similar (data not shown).

Mannose supplemented KI/KI mice have eye defects:

(a) Effect of mannose supplementation during conception and gestation: Surviving KI/KI pups born to mannose-fed dams and subsequently maintained on mannose had normal growth and life span. There were no visible abnormalities in any organ when KI/KI mice were dissected and compared with WT. The eyes were checked every week starting at week 2 when the mice just opened their eyes and continuing for up to 8 months. Approximately 45% of mannose supplemented pups displayed severe morphological eye defects (Table 6) that were clearly evident 2-8 weeks after birth. Most of the affected pups had either cloudy/opaque eyes (Fig.8b) or no eyes that appeared as shut-eye (Fig.8c) compared to normal eyes (Fig.8a). Histological analysis was done on the adult eyes isolated at 8 months. WT eyes showed normal development of all eye structures including lens, retinal-pigmented epithelium (RPE) and retina (Fig.8d). KI/KI mice that developed obvious eye defects by 3 weeks of age showed smaller eyecups, absence of the lens, disorganized retina, and clustering of pigmented cells inside the eye cup (Fig.8e). Mice with shut-eye developed much smaller eye-cups and had extensive hemorrhage with no eye structure remaining except for an eye socket-like structure containing pigmented tissue with vacuoles (Fig.8f,g). The identity of these cells is unknown, but markers for RPE progenitors – Mitf and Otx2 failed to stain the pigmented mass (data not shown). One KI/KI mouse supplemented with mannose since conception had a defective right eye and a seemingly normal left eye. However, when sacrificed at 8 months, the left eye also had a degenerating lens (Fig.8h).

(b) Effect of mannose on post-natal eye development in KI/KI mice: Since eye development continues up to 4 weeks post-birth, we supplemented KI/KI mice with 1 or 2% mannose after birth, starting at P1, where the development of the eye and lens is expected to be normal till birth. However, this set of mice also showed eye defects with 2% mannose supplementation, some of which were observed by 3 weeks, those exposed to 1% mannose did not (Table 6). The histologic examination at 8 months showed an eye with disintegrated lens, excess extracellular matrix (ECM), distorted retina and accumulated pigmented cells (Fig.8i), suggesting ill effects of P1 mannose supplementation. Some mice with mannose exposure also developed cloudy eyes later at approximately 3 months – with clear signs of cataract and a deteriorating lens and retina (Fig.8j). In this case, besides accumulation of ECM, the nucleus of the lens protruded out of the lens capsule and was vacuolated.

Vision of WT and KI/KI mice was checked by using an optometer with a motorized drum, painted with black and white strips. Mice with defective right eyes did not show any head turns during clockwise rotation and the

ones having defects in the left eye failed to show any head turns during counter-clockwise rotation (Supplemental Table 1). Mice with both eyes affected did not show any head turns in either direction. This data confirmed that the eyes, which developed defects either early on or later in life, were functionally impaired.
None of the KI/KI animals had eye defects when mannose was added to the drinking water at 6-8 weeks of age, which is 2-4 weeks after full eye development.

Our results here clearly suggest that mannose supplementation starting before conception or one day post-birth causes two separate, time-resolved types of eye pathology in KI/KI mice, which seemed to be rooted in altered mannose metabolism.

Mannose initiates ocular defects during embryogenesis: We could observe the eyes once mice opened them around 2 weeks. Eye development starts around E8.5 and continues until 4 weeks post-birth. We wanted to know if eye deterioration starts at embryonic stages or post birth in mice exposed to mannose *in utero*. We provided 2% mannose in KI/KI dam's drinking water during timed matings and monitored embryonic eye development at various stages by histology. At E10-11, WT mice develop an appropriate lens pit (Fig.9a), but KI/KI mice given mannose do not (Fig.9b). Instead they form smaller lens vesicles at E12-13 (Fig.9d) or none at all (Fig.9e). Wild-type mice had well formed lenses at E12-13 (Fig.9c), and both WT and KI/KI mice form a neuroepithelium and an outer layer of RPE. Some of the mannose-exposed eyes continue to develop with small lens vesicles or without any lens (E14-15) (Fig.9g, h) when compared to WT (Fig.9f). By E16-17, WT eye had a well-differentiated clear lens and a laminated retina with inner and outer layers (Fig.9i). Eyes from mannose-exposed mice were much smaller, have a neuroepithelium that lagged behind in its differentiation and mesenchymal cells from the surrounding area as well as blood cells that appeared to infiltrate the vacant area of the optic cup (Fig.9j, k). By E18-19, in some cases, the retina folded around in the vitreous space with an overproduction of retina cells and delayed differentiation. The optic cup of affected KI/KI eyes was significantly smaller than those of WT eyes at all embryonic stages (Fig.10). Some of the mannose-supplemented mice were then born with eyes that had a small, deteriorating cataractous lens (Fig.9p) or were devoid of lens (Fig.9q) and the optic cup was filled with different cell types, which further deteriorated with time (Fig.8e, g).

We assessed the effects of mannose on retinal development by using a series of retinal cell type specific antibodies. Pax-6 served as an early marker for retinal progenitors during neurogenesis. After the onset of retinal differentiation, it indicates ganglion and amacrine cells. In addition, we could specifically detect ganglion cells (Brn-3a), amacrine cells (AP-2), and photoreceptors (S-Opsin and M/L Opsin). We could detect

ganglion cells present in the ganglion cell layer (GCL), amacrine cells present in the inner nuclear layer (INL) and photoreceptors in the outer nuclear layer (ONL) that expanded their outer segments (OS) next to the RPE at the back of the eye in WT and KI/KI eyes at P28 (Fig.11a,b). The number of Brn-3a$^+$ ganglion cells was not affected (Fig.11b). However, there were significantly fewer AP-2$^+$ amacrine cells in the mature KI/KI eyes (Fig.11a,d) as well as at embryonic stage E18.5 (Fig.11c,d). Mannose may either partially impair differentiation of normal retina progenitor cells to amacrine cells in KI/KI embryonic eyes or lead to their apoptosis.

Our results clearly demonstrate that mannose-induced eye abnormalities in KI/KI embryos begin early in embryogenesis, starting with impaired lens formation and subsequently differentiation of some retinal cells required for further eye development. The results of our statistical analyses (Table 6) and histological examination of the eyes suggest that there is a variable penetrance of *Mpi* eye pathology.

Affected eyes have elevated mannose and Man-6-P levels. Eyes have the lowest MPI specific activity of all organs tested and this activity was reduced by 92% to 0.124 $\pm$ 0.025 nmol/min/mg in KI/KI animals (Table.3). Low MPI activity might render eyes more susceptible to adverse effects of mannose supplementation by accumulating Man-6-P. Man-6-P content of the eyes was similar in WT and KI/KI mice without mannose supplementation (Fig.12a). However, it increased 1.3-fold in the normal appearing KI/KI eyes and by 2.0 fold in the visibly cloudy eyes in 1 or 2% mannose-supplemented KI/KI mice (Fig.12a). We used GC-MS to check the levels of mannose, Man-6-P and mannitol in the affected and normal eyes of 1% mannose-supplemented KI/KI mice. Mannitol did not accumulate but mannose and Man-6-P levels were significantly higher in the affected eyes than in the normal eyes (Fig.12b). These results suggest that ongoing mannose consumption raises mannose and Man-6-P levels in KI/KI eyes and correlates with increased ocular abnormalities.

Discussion

There are nearly 100 known types of human glycosylation disorders. The CDG group comprises most of them. One of the major hurdles in studying these disorders is the lack of animal model systems. Mouse and rat mammalian models are closely related to humans and are widely used to study inherited human disorders. A few attempts have been made in the past to create knockout mouse models, however the models for MPI-CDG (CDG-Ib), PMM2-CDG (CDG-Ia), SRD5A3-CDG (CDG-Iq) and DPAGT1-CDG (CDG-1j) are embryonic lethal (3, 20–22) and those for MGAT2-CDG (CDG-IIa), SLC35C1-CDG (CDG-IIc) and β4GalT1-CDG (CDG-IId) have early post-natal lethality (23–26). These outcomes emphasize the importance of glycosylation

for early human development, but they cannot be used to model most aspects of the disease. Hypomorphic lines are more likely to mimic patient phenotypes.

We chose to create a murine line containing a mutation that generates a Y255C transition in MPI because preliminary experiments in cell lines showed that this line retains ~8-14% residual MPI activity. This amount of activity should ideally mimic residual activity seen in the patient who was a compound heterozygote for Y255C and I398T and retained 7% residual MPI activity. This patient was hypoglycemic, hyperinsulinemic, had hepatomegaly, elevated transaminase levels and had reduced factor XI, antithrombin III, protein S, and protein C levels (27).

Mpi is an essential, non-redundant gene in mice. Surprisingly, both hypomorphic lines with very low residual MPI activity and those with altered mannose metabolism grew normally and failed to mimic any of the broad array of symptoms of MPI-CDG patients. The activity was still sufficient for normal function in this strain. Limited outcrossing into a mixed 129/SV background also yielded no obvious pathological phenotype (data not shown).

We observed modest embryonic lethality in KI/KI mice that was presumably due to insufficient glycosylation. By analogy with mannose treatment of young MPI-CDG patients, we assumed that mannose provided prenatally would correct the slight embryonic lethality. The results were opposite to our expectations. Mannose supplementation caused a dose-dependent lethality during gestation in KI/KI mice. This was likely due to high local mannose or Man-6-P concentration that alters glucose metabolism at a crucial time during development. The results of earlier studies showed that mannose provided at 5 mM slowed rat embryo development in culture and showed impaired neural tube morphogenesis (28). The teratogenic effect on rat embryos was attributed to the impairment of glycolysis and the effects could be reversed by glucose. Mannose was also found to be toxic to honey bees because of Man-6-P accumulation (29). Alternatively, Man-6-P may inhibit processes mediated by Man-6-P receptors as expression of the two receptors is spatially and temporally regulated during mouse embryogenesis (30). One such example is proliferin, a placental growth and primary angiogenic factor expressed during mid-gestation (8-12 days) (31), which binds to Man-6-P receptor on fetal and maternal tissue. This binding is abolished by mannose, but Man-6-P is 1000 times more effective (half maximal effect at 10 μM) suggesting a very specific effect of Man-6-P on the proliferin binding to one of the Man-6-P receptors (32).

In survivors, prenatal mannose affected only eye development in KI/KI animals. This is most likely due to higher mannose levels and lower MPI activity in the eyes than in all other major organs. Approximately 45% animals developed ocular defects with varying degrees of severity, which suggests incomplete or reduced penetrance of the genetic mutation.

Histologic analysis of eyes during embryonic development indicates failure to form a normal lens pit. This deformity initiates a cascade resulting in the absence of a lens, which is crucial for continued eye morphogenesis (33–35). Eyes lacking a lens grow slower, fail to accumulate vitreous substance and are smaller (36, 37). Also, eyes devoid of a lens have a disorganized corneal endothelium and anterior segment (38). These findings suggest that extensive cross-talk occurs among the various cell types during eye development, with lens being a major player. We do not know at which stage the initiation event leading to collapse of eye structure occurs, however, we could see inhibition of lens vesicle formation as early as E10.

Galactosemic cataracts are generally caused by galactose and galactitol accumulation due to lower galactose metabolic enzymes (39, 40). Hyperglycemia also causes cataracts to develop in those with diabetes (41). Aldol reductase, an enzyme with low specificity causes polyol accumulation and is implicated in galactosemic and diabetic cataracts (42). Therefore, we expected an accumulation of mannitol in KI/KI eyes with mannose supplementation. However, mannitol did not accumulate despite elevated mannose levels in the affected/cloudy KI/KI eyes. The adverse effects are at least partially explained by the accumulation of mannose and Man-6-P in the affected KI/KI eyes. We also observed increased Man-6-P in KI/KI embryos, but were unable to measure it specifically in embryonic eyes. Our data clearly show adverse effects on lens and amacrine cells in the retina. Other cell types could also be affected via several different mechanisms. For example, phagocytosis of photoreceptor outer segments by retinal pigmented epithelium is mediated by mannose receptors on the apical side and is inhibited specifically by mannose and mannans (43, 44). Also, transforming growth factor-β (TGF-β, which is critical for eye development (45) and is expressed in lens fibers around E14.5 through E17.5 (46) could be affected. TGF-β precursor activation is specifically inhibited by Man-6-P prior to binding to its receptor but not by Man-1-P (47).

KI/KI mice were continuously exposed to mannose during conception, gestation and after birth. Therefore, we do not know the time frame during early development when embryos are most susceptible to mannose. The first indications of mannose-induced embryo demise and impaired lens development occur around E10.5. This coincides with the death of both previously reported *Mpi*-null and hypomorphic $Pmm2^{R137H/F118L}$ embryos (3, 19). All have placental abnormalities. Man-6-P accumulation in the *Mpi* null (3) and in mannose-exposed KI/KI

embryos presumably contributes to their death, while insufficient glycosylation is lethal for the *Pmm2*$^{R137H/F118L}$ embryos (19). Providing ~1% mannose in the drinking water of *Pmm2*$^{R137H/F118L}$ -bearing dams rescues insufficient glycosylation and ensures pup survival beyond weaning. Importantly, the same amount of mannose that rescues this strain is teratogenic or lethal in the KI/KI genotype. In both cases, the dams show only a nominal (1.4-1.7-fold) increase in their blood mannose concentration, suggesting that moderate changes in metabolite concentrations lead to drastic outcomes. These results underscore the importance of regulation of mannose concentration during embryonic development. Man-6-P is a common substrate for both MPI and PMM2. The ratio of PMM2:MPI activity determines the metabolic flux and steady state of Man-6-P (5). Imbalance of this ratio in *Mpi* hypomorphic embryos makes them incapable of coping with the increased mannose influx. Man-6-P was not reported in the *Pmm2*$^{R137H/F118L}$ embryos (19).

It is uncertain whether the results of mannose supplementation using *Mpi* in this study or *Pmm2* hypomorphic mice (19) can be extrapolated to humans. Based on the published results that mannose supplementation rescues *Mpi*-morpholino mediated knocked down in zebrafish embryos (MPI-CDG model) and reverses lethality of *Pmm2* hypomorphic mouse embryos (PMM2-CDG model) when started before conception and continued through gestation till birth, physicians might encourage mothers of MPI-CDG children to take mannose during a subsequent pregnancy to prevent symptoms that might develop during gestation. However, on the basis of our limited results, we strongly advise against this action. Similarly, we regard the recommendation made by an earlier publication (19) that mothers at-risk of having PMM2-CDG babies consume mannose during pregnancy to overcome the symptoms of PMM2-CDG *in utero*, as being highly premature because a narrow window of mannose metabolic flux may determine normal *vs.* pathologic state during embryogenesis as demonstrated in Fig.7a where there is a significant increase in Man-6-P levels even in WT mice supplemented on 2% mannose. A similar study to demonstrate toxicity in humans is not feasible.

Mannose is also widely sold as urinary tract health supplement. It is known to competitively inhibit binding of infectious *E.coli* to urinary tract of mice (48) and recently, the first human clinical trial showed mannose as an effective prophylactic agent with minimal side effects (49). The widespread use of mannose as a risk-free, internet-available, “natural glyconutrient” remedy for urinary tract infections underscores the need for caution, especially during pregnancy since the prevalence of MPI-CDG is unknown.

Bibliography

1. Niehues R., Hasilik M., Alton G., Körner C., Schiebe-Sukumar M., Koch H. G., Zimmer K. P., Wu R., Harms E., Reiter K., von Figura K., Freeze H. H., Harms H. K., Marquardt T. (1998) Carbohydrate-deficient

glycoprotein syndrome type Ib. Phosphomannose isomerase deficiency and mannose therapy. *J. Clin. Invest*. 101, 1414–1420.

2. De Lonlay P., Seta N. The clinical spectrum of phosphomannose isomerase deficiency, with an evaluation of mannose treatment for CDG-Ib. (2009) *Biochim. Biophys. Acta*. 1792, 841–3.

3. DeRossi C., Bode L., Eklund E. A., Zhang F., Davis J. A., Westphal V., Wang L., Borowsky A.D., Freeze H. H.. Ablation of mouse phosphomannose isomerase (Mpi) causes mannose 6-phosphate accumulation, toxicity, and embryonic lethality. (2006) *J Biol Chem*. 281, 5916–27.

4. Davis J. A., Wu X. H., Wang L., DeRossi C., Westphal V., Wu R., Alton G., Srikrishna G., Freeze H. H. (2002) Molecular cloning, gene organization, and expression of mouse Mpi encoding phosphomannose isomerase. *Glycobiology*, 12, 435–42.

5. Sharma V., Freeze H. H. (2011) Mannose efflux from the cells: a potential source of mannose in blood. *J Biol Chem.*, 286, 10193–200.

6. Sharma V., Ichikawa M., He P., Scott D. A., Bravo Y., Dahl R., Ng B. G., Cosford N. D., Freeze H. H. (2011) Phosphomannose isomerase inhibitors improve N-glycosylation in selected phosphomannomutase-deficient fibroblasts. *J Biol Chem*., 286, 39431–8.

7. Gracy R. W., Noltmann E. A. (1968) Studies on phosphomannose isomerase. I. Isolation, homogeneity measurements, and determination of some physical properties. *J Biol Chem*., 243, 3161–8.

8. Crossley J. R., Elliott R. B. (1977) Simple method for diagnosing protein-losing enteropathies. *Br Med J*., 1, 428–9.

9. Price N. P. J. (2004) Acylic sugar derivatives for GC/MS analysis of 13C-enrichment during carbohydrate metabolism. *Anal Chem.*, 76, 6566–74.

10. Donthi R. V., Epstein P. N. (2007) Altering and analyzing glucose metabolism in perfused hearts of transgenic mice. *Methods Mol Med*., 139, 151–61.

11. Zhu A. , Romero R. , Petty H. R. (2009) An enzymatic fluorimetric assay for glucose-6-phosphate: application in an in vitro Warburg-like effect. *Anal Biochem*., 388, 97–101.

12. Cline A., Gao N., Flanagan-Steet H., Sharma V., Rosa S., Sonon R., Azadi P., Sadler K. C., Freeze H. H., Lehrman M. A., Steet R. (2012) A zebrafish model of PMM2-CDG reveals altered neurogenesis and a substrate-accumulation mechanism for N-linked glycosylation deficiency. *Mol Biol Cell*., 23, 4175–87.

13. Chu J., Mir A., Gao N., Rosa S., Monson C., Sharma V., Steet R., Freeze H. H., Lehrman M. A., Sadler K. C. (2012) A zebrafish model of congenital disorders of glycosylation with phosphomannose isomerase deficiency reveals an early opportunity for corrective mannose supplementation. *Dis Model Mech*. 2012, 6, 95-105.

14. Halket J. M., Zaikin V. G. (2003) Derivatization in mass spectrometry--1. Silylation. *Eur J Mass Spectrom (Chichester, Eng)* 9, 1–21.

15. Michelakakis H., Moraitou M., Mavridou I., Dimitriou E. (2009) Plasma lysosomal enzyme activities in congenital disorders of glycosylation, galactosemia and fructosemia. *Clin Chim Acta*. 401, 81–3.

16. Marklová E, Albahri Z. (2007) Screening and diagnosis of congenital disorders of glycosylation. *Clin Chim Acta*., 385, 6–20.

17. Bode L., Salvestrini C., Park P. W., Li J. P., Esko J. D., Yamaguchi Y., Murch S., Freeze H. H. (2008) Heparan sulfate and syndecan-1 are essential in maintaining murine and human intestinal epithelial barrier function. *J Clin Invest*., 118, 229–38.

18. Davis J. A., Freeze H. H. (2001) Studies of mannose metabolism and effects of long-term mannose ingestion in the mouse. *Biochim Biophys Acta*.,1528, 116–26.

19. Schneider A., Thiel C., Rindermann J., DeRossi C., popovici D., Hoffmann G. F., Grone H. J., Korner C. (2011) Successful prenatal mannose treatment for congenital disorder of glycosylation-Ia in mice. *Nat Med*., 18(1):71–3.

20. Thiel C., Lübke T., Matthijs G., von Figura K., Körner C. (2006) Targeted disruption of the mouse phosphomannomutase 2 gene causes early embryonic lethality. *Mol Cell Biol*., 26, 5615–20.

21. Marek K. W., Vijay I. K., Marth J. D. (1999) A recessive deletion in the GlcNAc-1-phosphotransferase gene results in peri-implantation embryonic lethality. *Glycobiology*, 9, 1263–71.

22. Cantagrel V., Lefeber D. J., Ng B. G., Guan Z., Silhavy J. L., Bielas S. L., Lehle L., Hombauer H., Adamowicz M., Swiezewska E., De Brouwer A. P., Blümel P., Sykut-Cegielska J., Houliston S., Swistun D., Ali B. R., Dobyns W. B., Babovic-Vuksanovic D., van Bokhoven H., Wevers R. A., Raetz C. R., Freeze H. H., Morava E., Al-Gazali L., Gleeson J. G. (2010) SRD5A3 is required for converting polyprenol to dolichol and is mutated in a congenital glycosylation disorder. *Cell*. 142, 203–17.

23. Wang Y., Tan J., Sutton-Smith M., Ditto D., Panico M., Campbell R. M., Varki N. M., Long J. M., Jaeken J., Levinson S. R., Wynshaw-Boris A., Morris H. R., Le D., Dell A., Schachter H, Marth J. D. (2001) Modeling human congenital disorder of glycosylation type IIa in the mouse: conservation of asparagine-linked glycan-dependent functions in mammalian physiology and insights into disease pathogenesis. *Glycobiology* 11, 1051–70.

24. Hellbusch C. C., Sperandio M., Frommhold D., Yakubenia S., Wild M. K., Popovici D., Vestweber D., Gröne H. J., von Figura K., Lübke T., Körner C. (2007) Golgi GDP-fucose transporter-deficient mice mimic congenital disorder of glycosylation IIc/leukocyte adhesion deficiency II. *J Biol Chem*., 282, 10762–72.

25. Lu Q., Hasty P., Shur B. D. (1997) Targeted mutation in beta1,4-galactosyltransferase leads to pituitary insufficiency and neonatal lethality. *Dev Biol*., 181, 257–67.

26. Asano M, Furukawa K, Kido M, Matsumoto S, Umesaki Y, Kochibe N, Iwakura Y. (1997) Growth retardation and early death of beta-1,4-galactosyltransferase knockout mice with augmented proliferation and abnormal differentiation of epithelial cells. *EMBO J*., 16, 1850–7.

27. de Lonlay P., Cuer M., Vuillaumier-Barrot S., Beaune G., Castelnau P., Kretz M., Durand G., Saudubray J. M., Seta N. (1999) Hyperinsulinemic hypoglycemia as a presenting sign in phosphomannose isomerase deficiency: A new manifestation of carbohydrate-deficient glycoprotein syndrome treatable with mannose. *J Pediatr*., 135, 379–83.

28. Buchanan T., Freinkel N., Lewis N. J., Metzger B. E., Akazawa S. (1985) Fuel-mediated teratogenesis. Use of D-mannose to modify organogenesis in the rat embryo in vivo. *J Clin Invest*., 75, 1927–34.

29. Sols A., Cadenas E., Alvarado F. (1960) Enzymatic basis of mannose toxicity in honey bees. *Science*. 131, 297–8.

30. Matzner U., von Figura K., Pohlmann R. (1992) Expression of the two mannose 6-phosphate receptors is spatially and temporally different during mouse embryogenesis. *Development*., 114, 965–72.

31. Jackson D., Volpert O. V., Bouck N., Linzer D. I. (1994) Stimulation and inhibition of angiogenesis by placental proliferin and proliferin-related protein. *Science*, 266, 1581–4.

32. Lee S. J., Nathans D. (1988) Proliferin secreted by cultured cells binds to mannose 6-phosphate receptors. *J Biol Chem*., 263, 3521–7.

33. Genis-Galvez J. M. (1966) Role of the lens in the morphogenesis of the iris and cornea. *Nature*. 210, 209–10.

34. Breitman M. L., Bryce D. M., Giddens E., Clapoff S., Goring D., Tsui L. C., Klintworth G. K., Bernstein A. (1989) Analysis of lens cell fate and eye morphogenesis in transgenic mice ablated for cells of the lens lineage. *Development.* 106, 457–63.

35. Yamamoto Y., Jeffery W. R. (2000) Central Role for the Lens in Cave Fish Eye Degeneration. 289, 631–633.

36. Coulombre A. J., Coulombre J. L. Lens Development. I. Role of the lens in eye growth. (1964) *J Exp Zool*., 156, 39–47.

37. Coulombre A. J., Herrmann H. (1965) Lens development. 3. Relationship between the growth of the lens and the growth of the outer eye coat. *Exp Eye Res*., 4, 302–11.

38. Beebe D. C., Coats J. M. (2000) The lens organizes the anterior segment: specification of neural crest cell differentiation in the avian eye. *Dev Biol*., 220, 424–31.

39. Kinoshita J. H.(1965) Cataracts in galactosemia. The Jonas S. Friedenwald Memorial Lecture. *Invest Ophthalmol*., 4, 786–99.

40. Gitzelmann R., Curtius H. C., Schneller I. (1967) Galactitol and galactose-1-phosphate in the lens of a galactosemic infant. *Exp Eye Res*., 6, 1–3.
41. Varma S. D., Schocket S. S., Richards R. D. (1979) Implications of aldose reductase in cataracts in human diabetes. *Invest Ophthalmol Vis Sci*., 18, 237–41.
42. Dvornik E., Simard-Duquesne N., Krami M., Sestanj K., Gabbay K. H., Kinoshita J. H., Varma S. D., Merola L. O. (1973) Polyol accumulation in galactosemic and diabetic rats: control by an aldose reductase inhibitor. *Science*, 182, 1146–8.
43. Boyle D., Tien L. F., Cooper N. G., Shepherd V., McLaughlin B. J. (1991) A mannose receptor is involved in retinal phagocytosis. *Invest Ophthalmol Vis Sci*., 32, 1464–70.
44. Wilt S. D., Greaton C. J., Lutz D. A., McLaughlin B. J. (1999) Mannose receptor is expressed in normal and dystrophic retinal pigment epithelium. *Exp Eye Res*. 69, 405–11.
45. Saika S. (2006) TGFbeta pathobiology in the eye. *Lab Invest*., 86, 106–15.
46. Pelton R. W., Saxena B., Jones M., Moses H. L., Gold L. I. (1991) Immuno-histochemical localization of TGF beta 1, TGF beta 2, and TGF beta 3 in the mouse embryo: expression patterns suggest multiple roles during embryonic development. *J Cell Biol*., 115, 1091–105.
47. Dennis P. A., Rifkin D. B. (1991) Cellular activation of latent transforming growth factor beta requires binding to the cation-independent mannose 6-phosphate/insulin-like growth factor type II receptor. *Proc Natl Acad Sci U S A*., 88, 580–4.
48. Aronson M., Medalia O., Schori L., Mirelman D., Sharon N., Ofek I. (1979) Prevention of colonization of the urinary tract of mice with Escherichia coli by blocking of bacterial adherence with methyl alpha-D-mannopyranoside. J Infect. Dis., 139, 329-32.
49. Kranjcec B., Papes D., Altarac S. (2013) D-mannose powder for prophylaxis of recurrent urinary tract infections in women: a randomized clinical trial. World J Urol., Apr 30 [Epub ahead of print].

Acknowledgements

This work was supported by grants from the National Institutes of Health (R01-DK55615), the Children's Heart Fund and the Rocket Fund to HHF. We appreciate Dr. Peter Westenskow at The Scripps Research Institute (TSRI) for sharing some of the antibodies. We also thank Dr. Amanda Roberts at TSRI's mouse behavioral assessment core for providing access to the optic drum.

We greatly appreciate Guillermina Garcia and Robbin Newlin in SBMRI's histology core facility for their exceptional technical support with histology. We thank SBMRI animal facility's staff for setting up the mouse breeding and taking care of our animals and Buddy Charbono for his technical support. We also acknowledge technical support provided by Jamie Smolin in our laboratory.

Figure Legends

Scheme.1. Mannose Metabolic pathway. Man, mannose; Glc, glucose; HK, hexokinase; MPI, phosphomannose isomerse; PMM2, phosphomannomutase2; GDP-man, GDP-mannose, Dol-P-Man, dolichol phosphate mannose; LLO, lipid linked oligosaccharide.

Fig.1. MPI activity and antigen in various organs. Organ lysates were prepared from frozen tissue of three mice each as described in methods. (a) MPI activity was determined in duplicate for each sample and results are presented as the percentage of activity relative to that of WT control mice (100%). Error bars represent standard deviation of the mean of three replicates. White bars: KI/KI, Black bars – KI/KO. (b) Organ lysates from three mice were immunoblotted using anti-MPI antibody. % Represents intensity of the KI/KI and KI/KO protein bands relative to that of WT as calculated by Image J software.

Fig.2. [2-^{3}H]-Mannose labeling of fibroblasts and mice. Fibroblasts from mouse embryos (a) or human fibroblasts (b) were labeled in duplicate with [2-^{3}H]-Mannose and radiolabel was measured in TCA precipitable proteins. Mice were injected with 50 μCi [2-^{3}H]-Mannose and blood was collected at different times. Calculated $^{3}H_2O$ (c) and TCA precipitable ^{3}H-radiolabeled glycoproteins (d). Data shown are the mean of 3 mice in each group and error bars represent standard deviation. (e) Organ explants from WT and KI/KI mice were labeled with 50 μCi/ml [2-^{3}H]-Mannose and radiolabel was measured in glycoproteins precipitated with TCA. Inset shows the magnified view of the selected organs.

Fig.3. Embryo survival. Timed matings were set up and dams were provided with 5% mannose in drinking water during gestation. In vivo imaging was performed to monitor the pregnancies. The data shown are the mean of 5 experiments. Error bars indicate standard deviation.

Fig.4. Embryo demise and placental abnormalities with 5% mannose supplentation. WT and KI/KI dams were provided 5% mannose during gestation. At E13.5, dissections were performed to isolate embryos and placentae. (a) WT placenta, (b) WT embryo and (c) KI/KI placenta and embryo. Placentae were fixed and sections were stained with hematoxylin-eosin (H&E) stain (d) WT (e) KI/KI. Panels on the right side in (d) and (e) show the magnified view of the placenta. La = Labyrinth, Sp = Spongiotrophoblast, GC = Giant cells.

Fig.5. Placental size and embryo development with 2% mannose supplementation. Timed matings were set up and dams were provided 2% mannose in drinking water during gestation. (a) At different embryonic stages, placentae were fixed and sectioned. Diameter of the placenta was measured and plotted. Each symbol represents an individual placenta. (b and c) At E 8.5, whole uterus was fixed and the sections were stained with H&E to visualize embryos in utero. * ($p < 0.05$), ** ($p < 0.005$).

Fig.6. Serum mannose analysis. Concentration of mannose in serum from WT and KI/KI was determined by GC-MS as described in methods. * $p < 0.05$.

Fig.7. Man-6-P determination. Embryos (a) and placentae (b) were isolated at E11.5 from at least two different dams with or without mannose supplementation and Man-6-P was determined. Each symbol represents an individual embryo/ placenta. (* $p < 0.05$, ** $p < 0.005$)

Fig.8. Appearence and histological images of adult mice eyes. (a) Normal eye (b) Cloudy eye and (c) No eye phenotype. (d - j) is H&E stains of fixed eyes. (d) normal WT eye. (e - h) Representative KI/KI eyes of mice who were maintained on mannose after being born to mannose-fed dams during conception and gestation (e) an eye with cloudiness evident at age 3 weeks has no lens, distorted retina and a cluster of pigmented cells (f) absence of an eye since birth shows as a small eye socket filled with vacuoles (g) magnified view of f. (h) an eye which appeared normal on physical examination showed deteriorating lens when sectioned and stained with H&E at 8 months. (i-j) Mannose supplementation was started at P1 (i) an eye that showed cloudiness at age 3 weeks has disintegrating lens and retina and infiltration of pigmented cells. (j) an eye that turned cloudy at age 3 months showing disintegrating lens. Scale bar length is indicated in mm or mm. L = Lens, R = Retina, C = Cornea, RPE = Retinal Pigmented Epithelium, PC = Pigmented Cells, ES = Eye Socket, V = Vacuole, Ch -

Choroid, ECM = Extracellular matrix, OS = Optic stalk, LR = Lens Remanants, LN = Lens Nucleus, Ca = Cataract.

Fig.9. Eyes at various developmental stages. Timed matings were set up and the dams were provided 2% mannose throughout gestation. At indicated days, the embryos were harvested and fixed. Paraffin sections were stained with H&E. The panels depict the histology of the eyes at various embryonic stages. WT normal eyes (a, c, f, i, l, o), KI/KI eyes with affected lens (b, d, g, j, m, p) and KI/KI eyes with no lens (e, h, k, n, q). OC =optic cup, LV = lens vesicle, NE - neuroepithelium, OS = optic stalk, R = retina, L = lens,R = retina, RPE - retinal pigment epithelium, Ca = Cataract, PC = pigmented cells. Magnification is the same for WT and KI/KI at each development stage, although it varies amongst stages, high (10-20X) for early embryonic stages and low (3.1-5X) for later embryonic stages and post-birth. Scale-bar length is 100 μm for (a) - (h), 400 μm for (i) - (n) and 1 mm for (o) - (q).

Fig.10. Optic cup measurement. Length of the cross-section of the optic cup of the fixed H&E stained eyes was measured by using Aperio software. *** ($p < 0.0005$), **** ($p < 0.0001$).

Fig.11. Immunofluorescence of WT and KI/KI eye sections: (a) staining with AP-2, an amacrine cell marker (in red) in the inner nuclear layer and M/L opsin (for red and green opsins), a cone photoreceptor cell marker (in green) for outer segments on P28 WT and KI/KI eyes. Scale bar is 100 μm for both panels. (b) staining with Brn3a, a ganglion cell marker (in red) in the GCL, and S opsin, a blue opsin cone photoreceptor cell marker (in green) in the outer segments of P28 WT and KI/KI sections. Scale bar is 100μm for both panels. (c) staining with Pax6, a ganglion and amacrine cell marker, (in green) and AP-2, an amacrine specific cell marker (in red) on E18.5 WT and KI/KI eyes. An amplification of boxed areas is shown on the right side of the panel. GCL: Ganglion Cell Layer; IPL: Inner Plexiform Layer; INL:Inner Nuclear Layer; OPL: Outer Plexiform Layer; ONL: Outer Nuclear Layer; Photoreceptor OS: Outer Segments. (d) Image J software was used to count the number of AP2 immunopositive cells from the posterior region of two different 40X confocal images from three different eyes and calculate the mean. The error bars represent standard deviation. **$p < 0.005$, ****$p < 0.0001$.

Fig.12. Measurement of metabolites in the eyes. (a) A coupled fluorescent assay was used to measure the concentration of Man-6-P in the eyes of WT and KI/KI mice supplemented with or without mannose. Status of the eye is represented by N = not affected, C = Cloudy. (b) Mannose, Man-6-P and mannitol concentrations were estimated by GC-MS of the normal and affected eyes of mannose fed KI/KI mice. Data shown are the mean of 5 mice and error bars represent SEM. ns = not significant, * ($p < 0.05$), ** ($p < 0.005$), *** ($p < 0.001$).

Table 1. MPI residual activity and antigen in mpi-null SEY6210delpmi40::URA3 yeast strain complemented with mutant mpi constructs.

MPI mutations	Residual MPI Protein (%)	Residual MPI activity (%)
WT	100	100
S102L	0	0.59
D131N	0	7.3
M138T	53.0	82.4
R152Q	83.1	99.7
R219Q	58.7	38.7
Y255C	24.9	12.3
I398T	101.2	109
R418H	66.2	65.3

Table.2. Heterozygous crosses [KI/+ x KI/+]. Data from 70 litters.

Genotype =>	WT (+/+)	Het (KI/+)	KI/KI
Number of mice	133	303	115
Predicted (%)	25	50	25
Observed (%)	24.1	54.9	20.8
p-value	0.187	0.830	0.004

Table.3. MPI specific activity in various organs. The data is an average of three mice with standard deviation. nd = not determined

	WT (nmol/mg/min)	KI/KI (nmol/mg/min)	KI/KO (nmol/mg/min)
Embryos (E11.5)	24.6±1.6	1.6±0.32	nd
Placenta (E11.5)	22.1±6.9	1.5±0.15	nd
Small Intestine	20.5±0.6	0.51±0.29	0.14±0.20
Kidney	19.7±0.9	1.20±0.14	0.57±0.08
Colon	16.8±2.7	1.46±0.53	0.92±0.18
Heart	14.9±2.1	2.80±0.6	1.4±0.01
Liver	8.3±0.9	0.25±0.03	0.04±0.005
Lung	8.4±2.3	0.68±0.21	0.32±0.18
Spleen	7.5±0.2	0.42±0.15	0.28±0.06
Eyes	1.5±0.2	0.12±0.02	nd

Table.4. Heterozygous breedings with mannose supplementation. n = number of litters

Heterozygous crosses	KI/+ x KI/+ (No Mannose)			KI/+ x KI/+ (5% Mannose)		
Average Litter Size	8.0 ± 1.7 (n=14)			6.0 ± 2.3 (n=6)		
% survival to weaning	84.8			94.4		
Progeny genotype	+/+	KI/+	KI/KI	+/+	KI/+	KI/KI
Number of progeny	29	49	17	14	20	0
% of each progeny	31	52	18	41	59	0
p value	0.26	0.26	0.04	0.12	0.44	-

Table.5. Homozygous breedings with mannose supplementation. p value signifies differences between WT and KI/KI for each supplement.

Mannose in the drinking water (%)	Average Litter size			Survival to weaning (%) n = no. of litters		
	WT	KI/KI	P value	$WT_{(n)}$	$KI/KI_{(n)}$	P value
0	8.6±1.8	7.5±2.0	0.01	90 (46)	84 (33)	0.13
1	8.0±1.3	5.3±1.0	0.01	92 (8)	61 (17)	0.001
2	9.6±1.3	5.4±3.9	0.005	84 (11)	33 (9)	0.02
5	6.7±1.2	0.0	-	15 (3)	0.0 (5)	-

Table.6. Mannose-supplemented mice develop eye defects.

% mannose	Mannose provided	WT			KI/KI				
		Total mice	Mice with eye defects	% affected mice	Total mice	Mice with eye defects	% affected mice	Early defects (2-8 wks)	Late defects (> 8 wks)
1	conception	55	1	1.8	49	23	46.9	16	7
2	conception	88	1	1.1	20	9	45.5	9	0
1	post-birth (P1)	30	0	0	26	1	3.8	1	0
2	post-birth (P1)	36	0	0	20	9	45	5	4
1	6 weeks	14	0	0	14	0	0	-	-
2	6 weeks	14	0	0	14	0	0	-	-

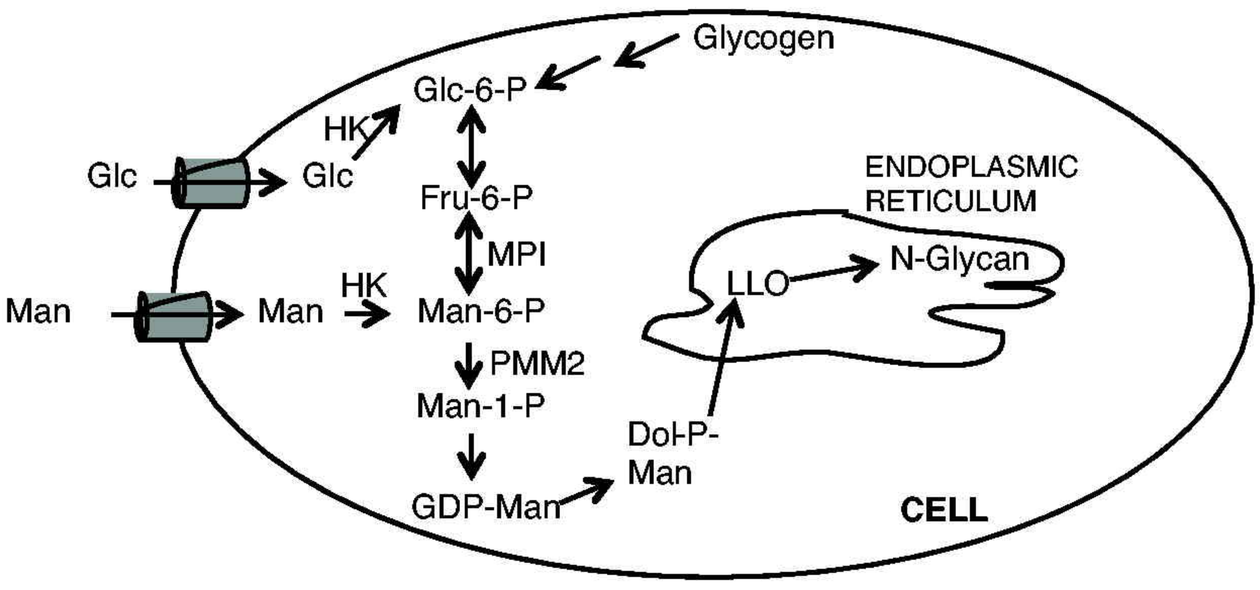
Glycogen
Glc-6-P
HK
Glc
Glc
Fru-6-P
MPI
HK
Man
Man
Man-6-P
PMM2
Man-1-P
GDP-Man
Dol-P-
Man
ENDOPLASMIC
RETICULUM
LLO
N-Glycan
CELL

Scheme.1

Figure.1

(a)

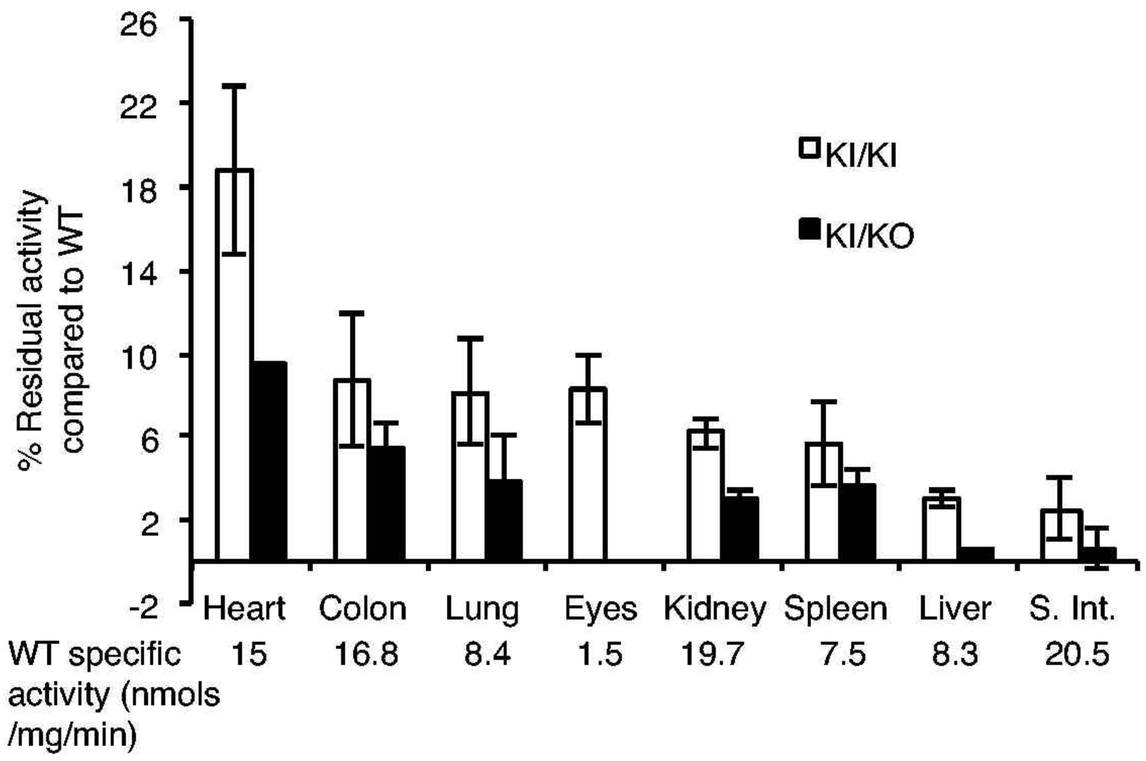
26
22
18
14
10
6
2
-2
% Residual activity compared to WT
KI/KI
KI/KO
Heart
Colon
Lung
Eyes
Kidney
Spleen
Liver
S. Int.
WT specific activity (nmols /mg/min)
15
16.8
8.4
1.5
19.7
7.5
8.3
20.5

(b)

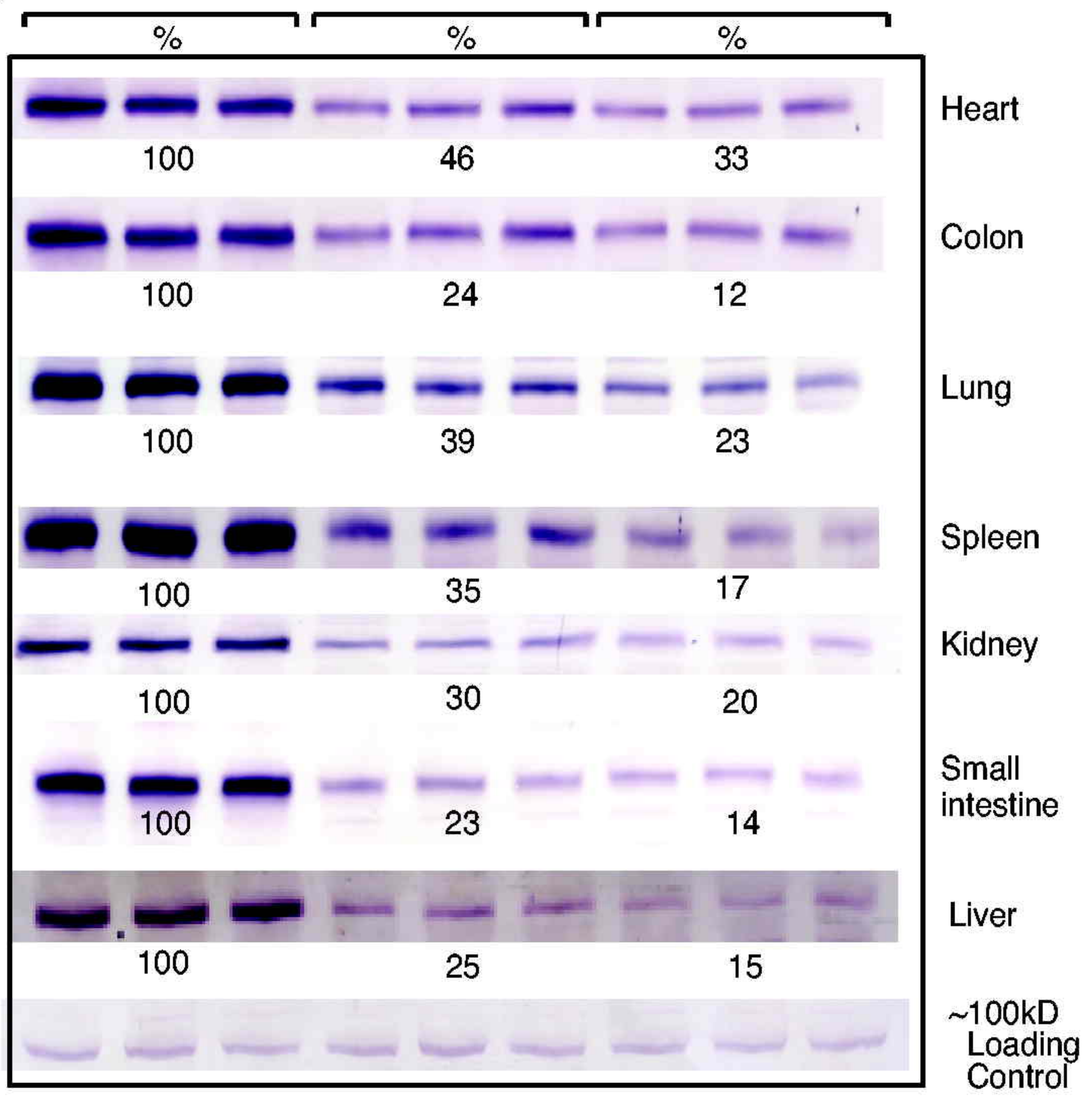
WT
KI/KI
KI/KO
%
%
%
Heart
100
46
33
Colon
100
24
12
Lung
100
39
23
Spleen
100
35
17
Kidney
100
30
20
Small intestine
100
23
14
Liver
100
25
15
~100kD Loading Control

Figure.2

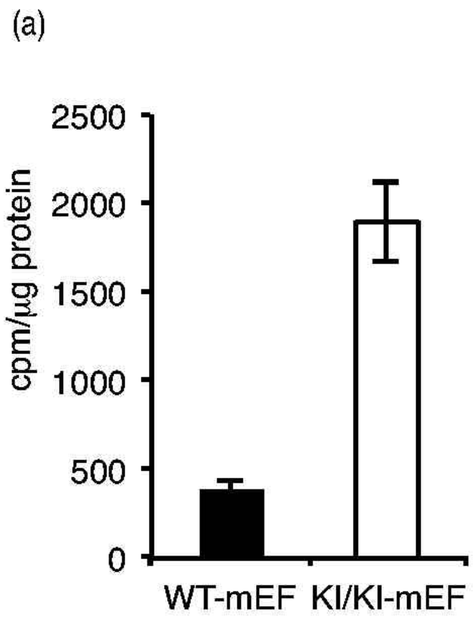
(a)
2500
2000
1500
1000
500
0
cpm/µg protein
WT-mEF
KI/KI-mEF

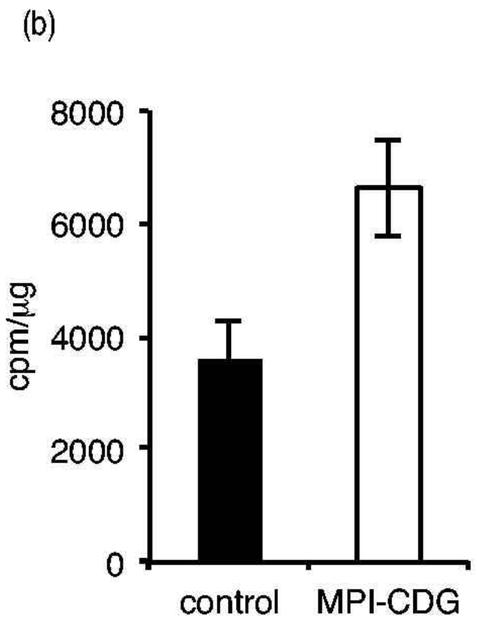
(b)
8000
6000
4000
2000
0
cpm/µg
control
MPI-CDG

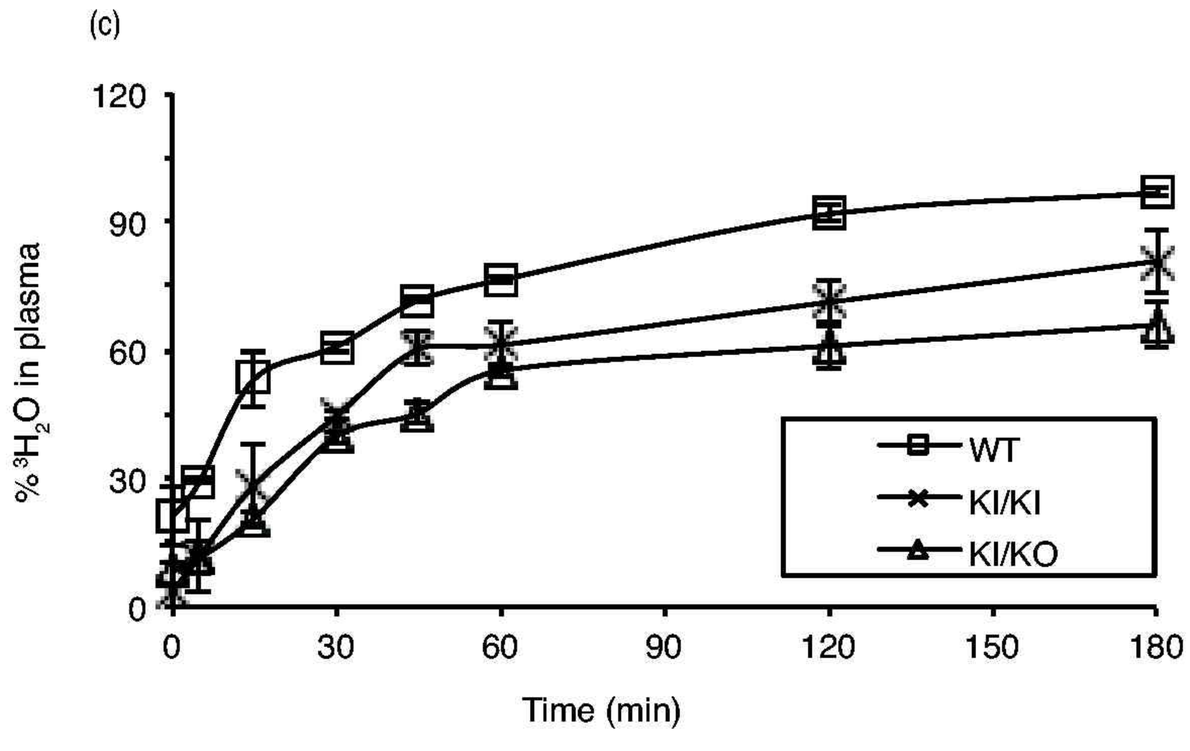
(c)
120
90
60
30
0
% 3H2O in plasma
0
30
60
90
120
150
180
Time (min)
WT
KI/KI
KI/KO

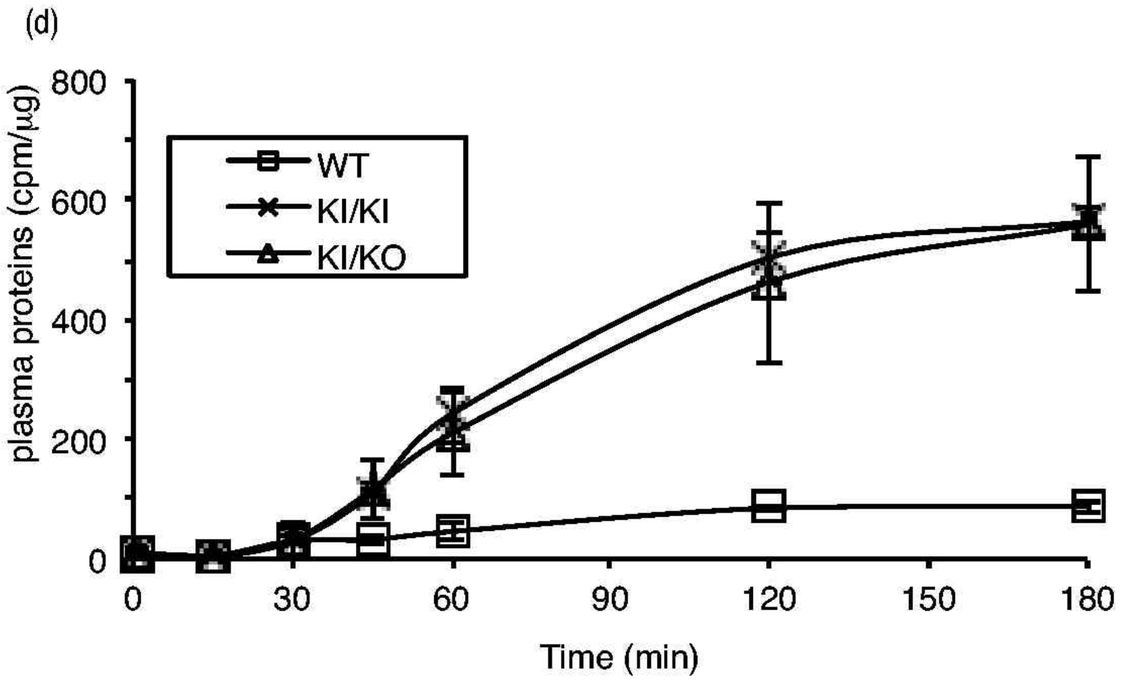
(d)
800
600
400
200
0
plasma proteins (cpm/µg)
WT
KI/KI
KI/KO
0
30
60
90
120
150
180
Time (min)

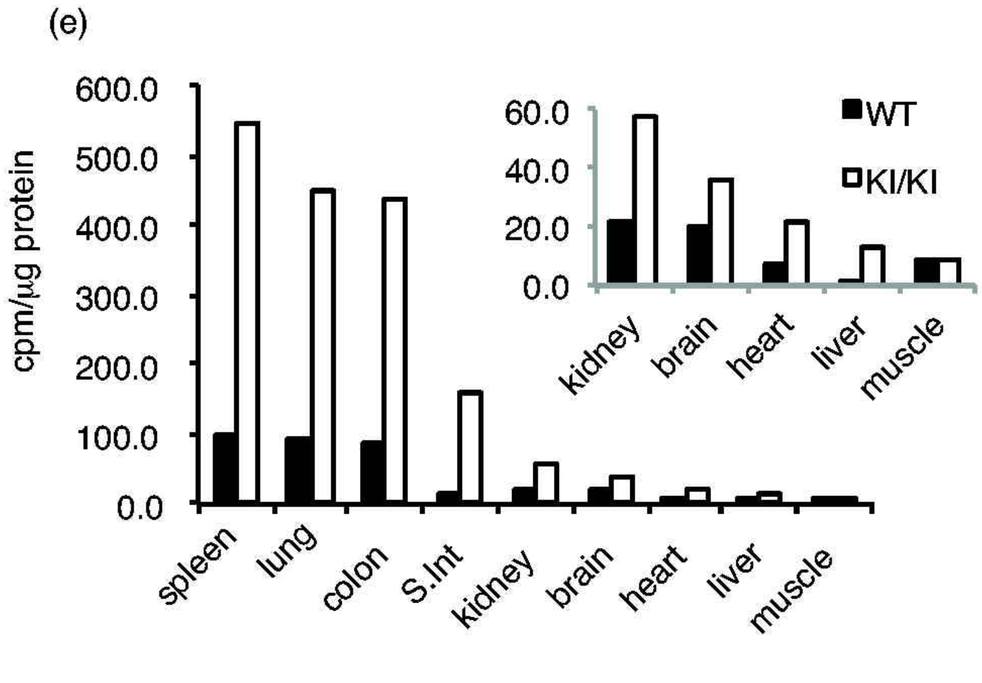
(e)
600.0
500.0
400.0
300.0
200.0
100.0
0.0
cpm/µg protein
spleen
lung
colon
S.Int
kidney
brain
heart
liver
muscle
60.0
40.0
20.0
0.0
WT
KI/KI
kidney
brain
heart
liver
muscle

Figure.3

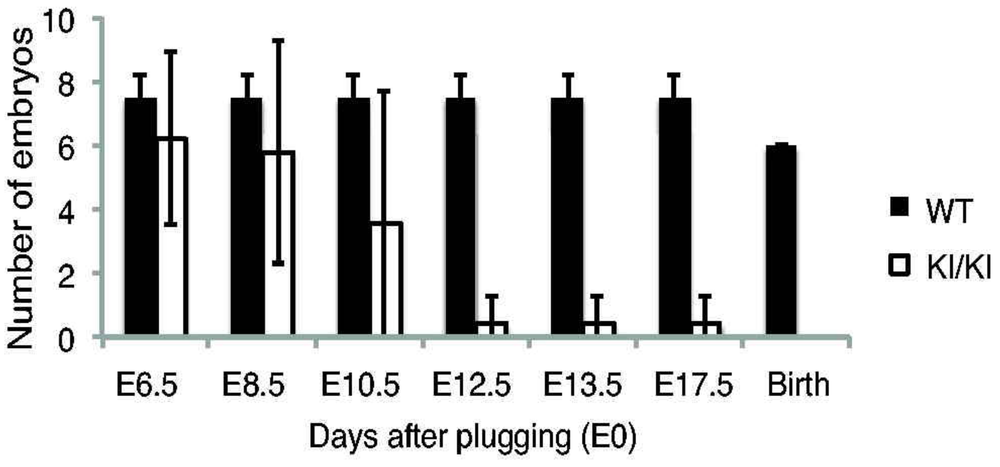
Number of embryos
10
8
6
4
2
0
E6.5
E8.5
E10.5
E12.5
E13.5
E17.5
Birth
Days after plugging (E0)
WT
KI/KI

Figure 4

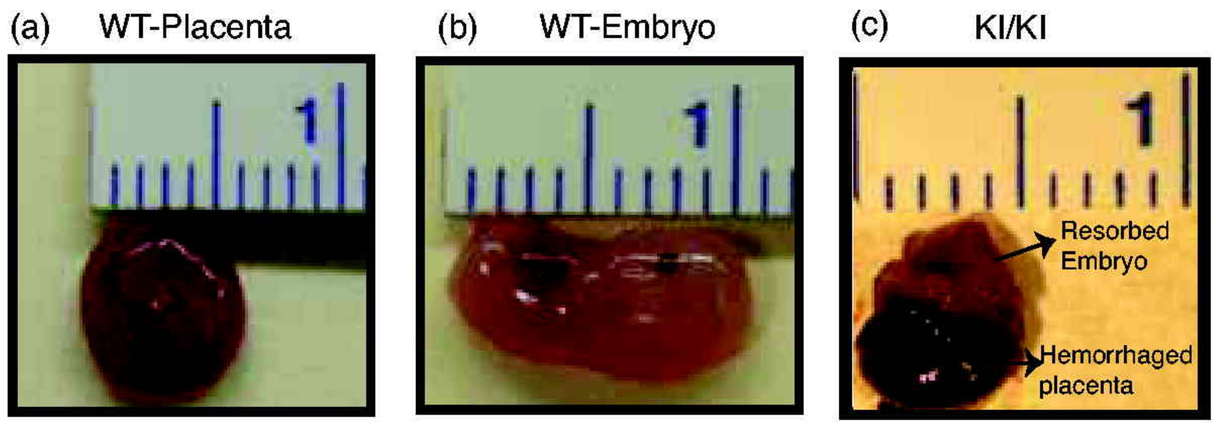
(a) WT-Placenta
(b) WT-Embryo
(c) KI/KI
1
1
1
Resorbed Embryo
Hemorrhaged placenta

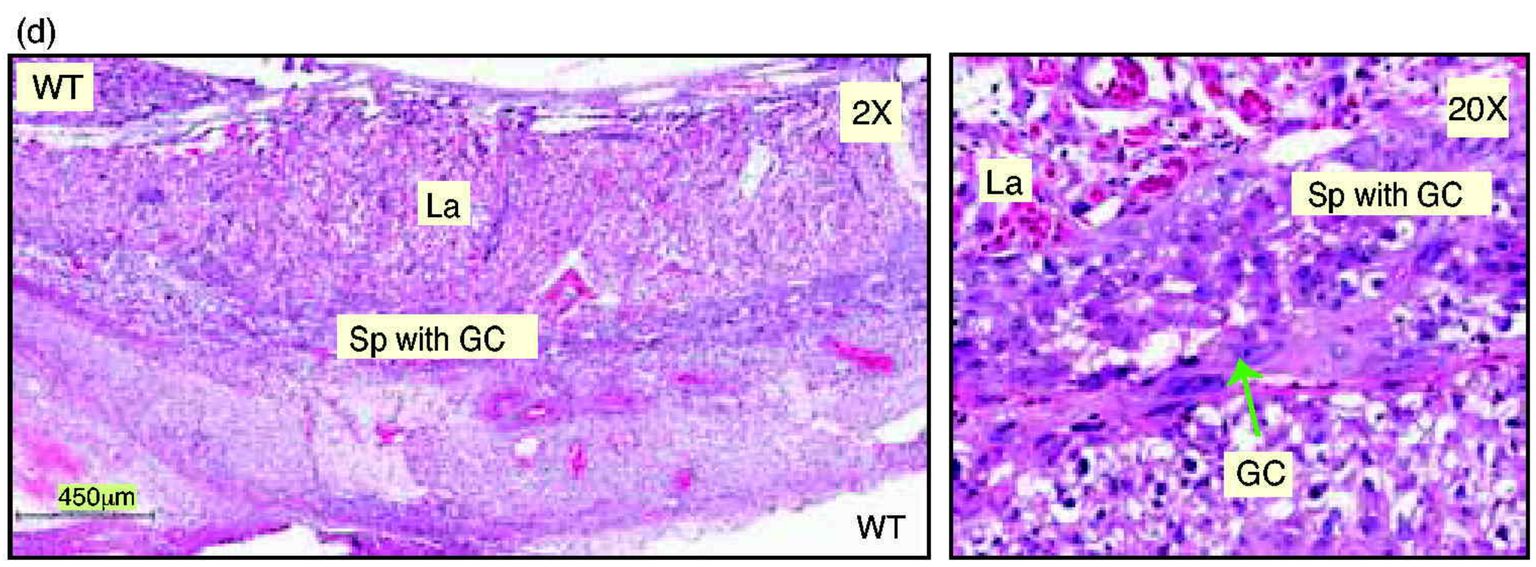
(d)
WT
2X
La
Sp with GC
450μm
WT
20X
La
Sp with GC
GC

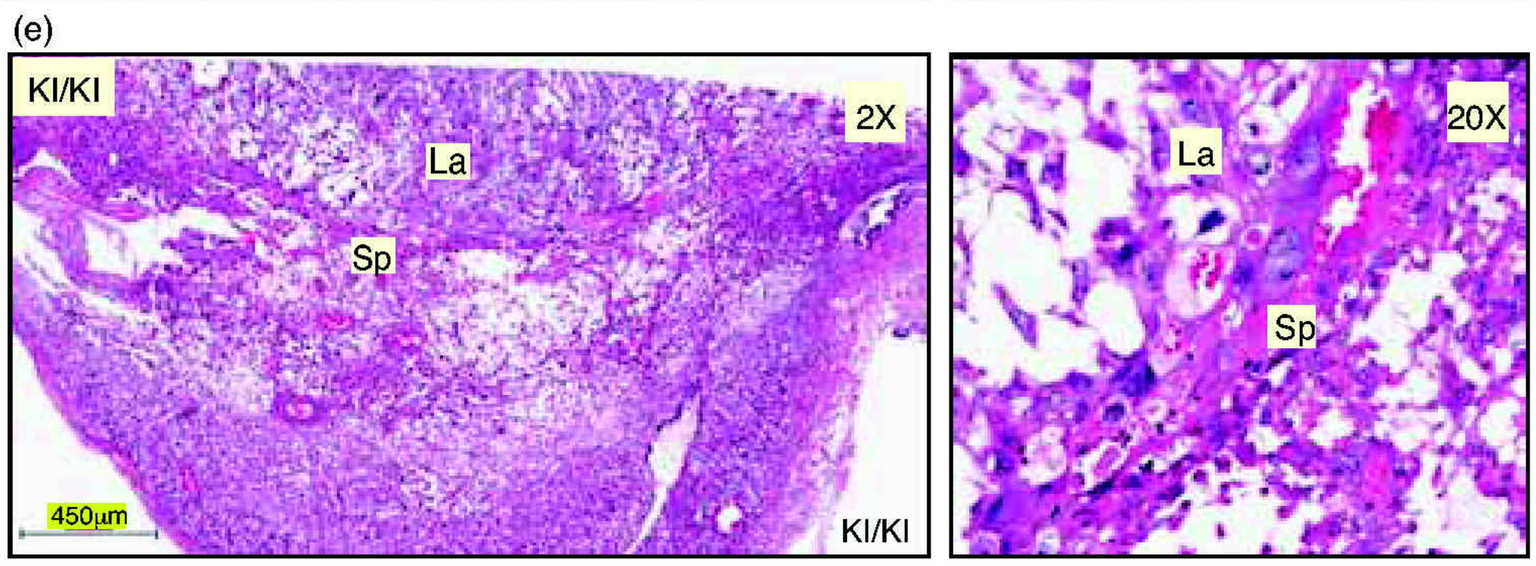
(e)
KI/KI
2X
La
Sp
450μm
KI/KI
20X
La
Sp

Figure.5

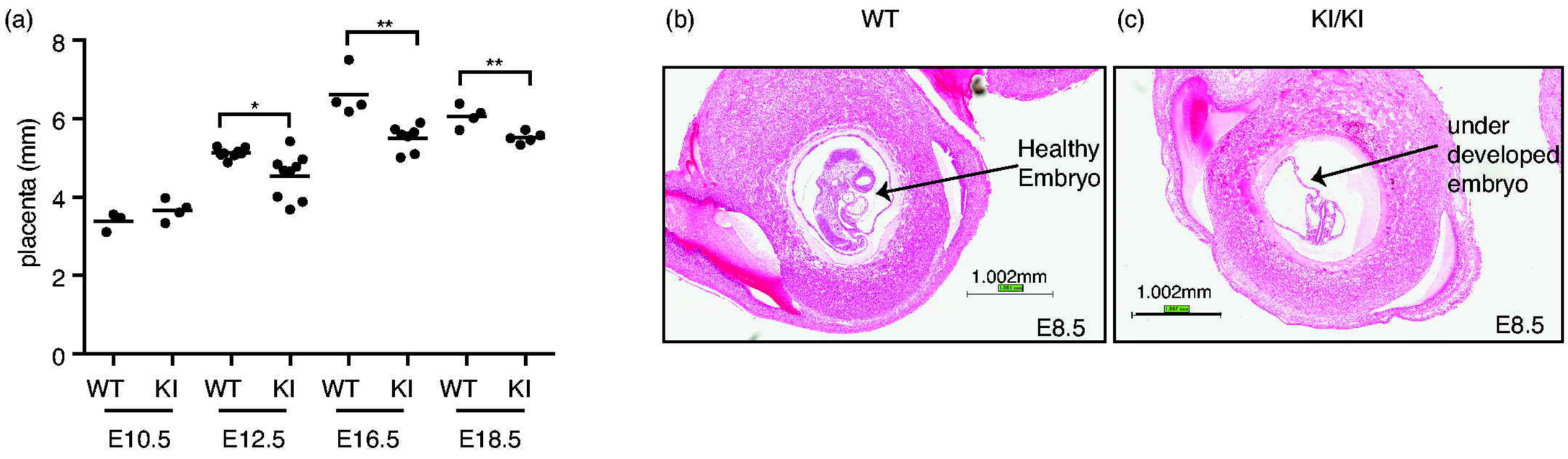
(a)
placenta (mm)
0
2
4
6
8
*
**
**
WT
KI
WT
KI
WT
KI
WT
KI
E10.5
E12.5
E16.5
E18.5
(b)
WT
Healthy
Embryo
1.002mm
E8.5
(c)
KI/KI
under
developed
embryo
1.002mm
E8.5

Figure.6

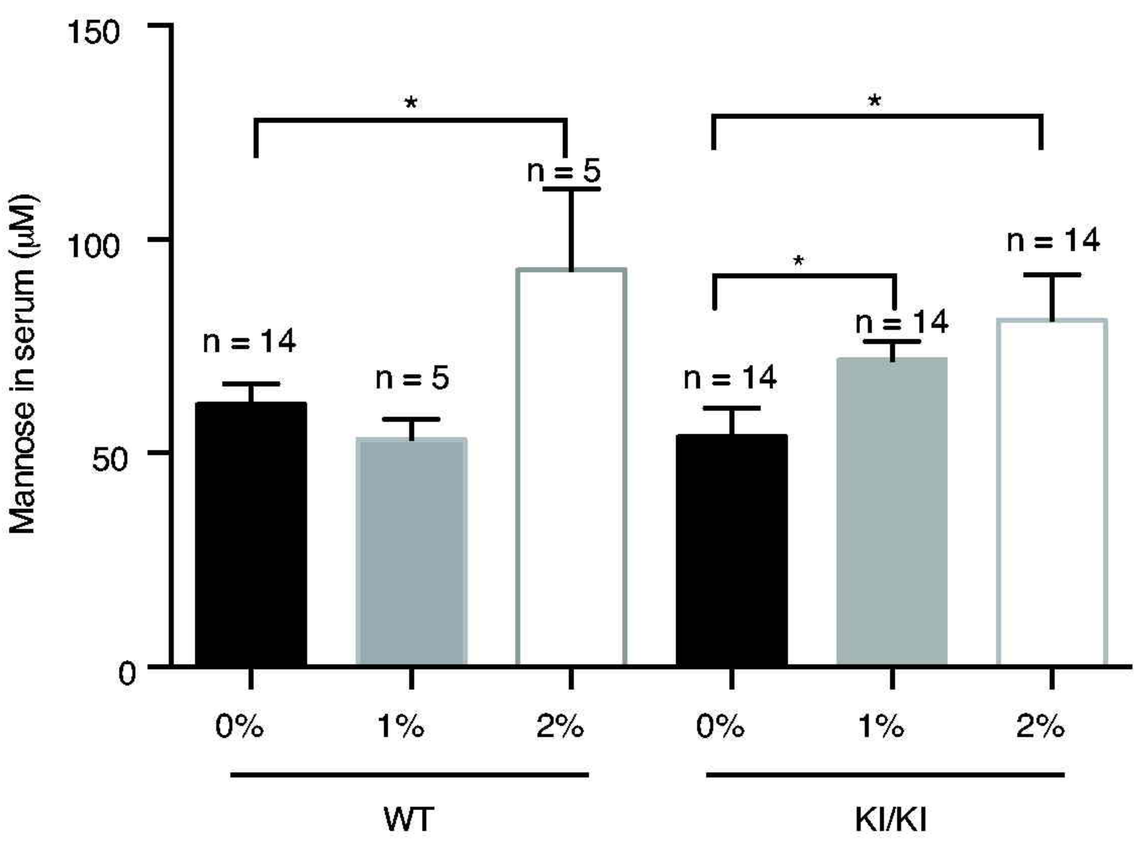
150
100
50
0
Mannose in serum (μM)
*
*
*
n = 5
n = 14
n = 5
n = 14
n = 14
n = 14
0%
1%
2%
0%
1%
2%
WT
KI/KI

Figure.7

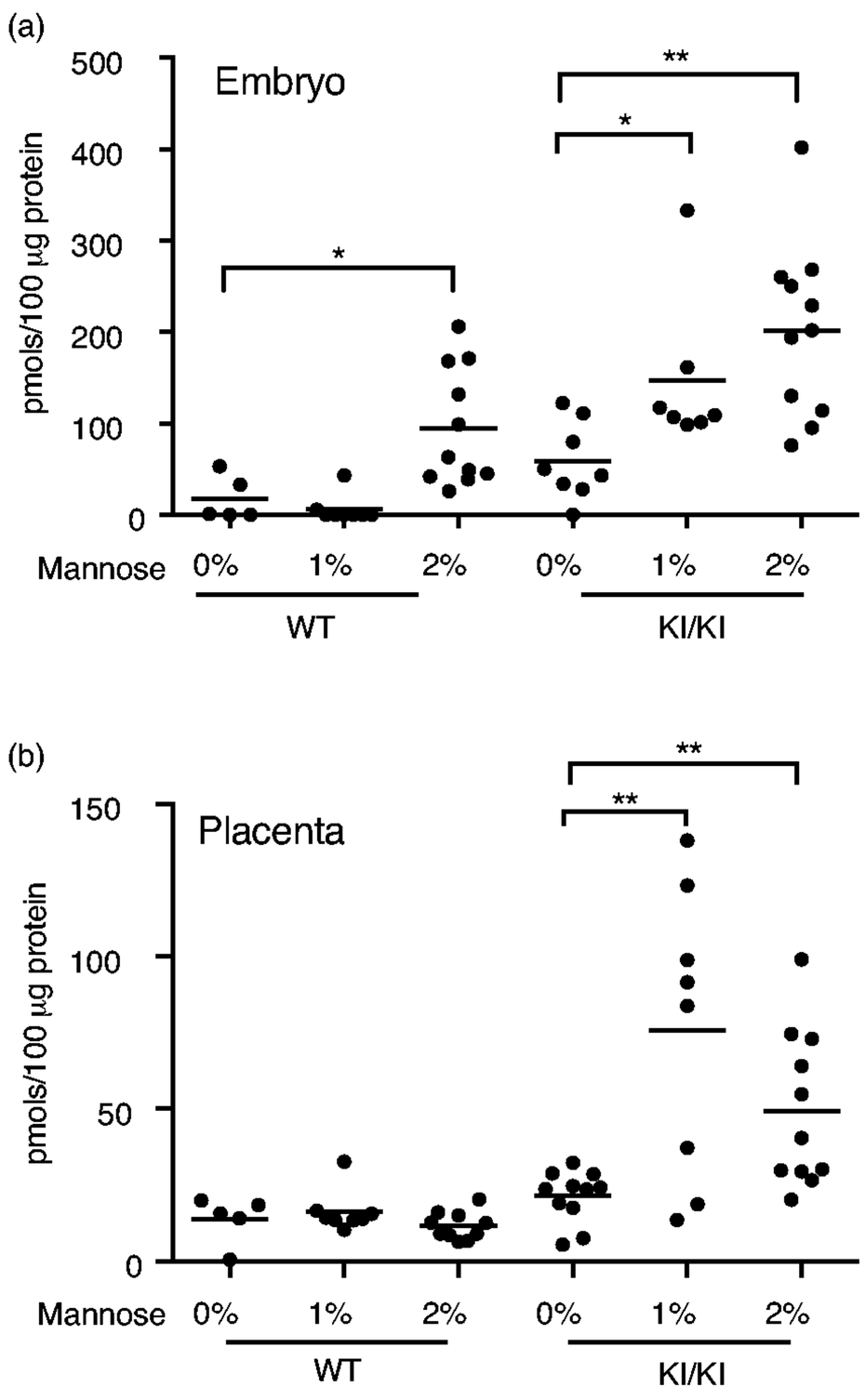
(a)
Embryo
pmols/100 µg protein
500
400
300
200
100
0
**
*
*
Mannose
0%
1%
2%
0%
1%
2%
WT
KI/KI
(b)
Placenta
pmols/100 µg protein
150
100
50
0
**
**
Mannose
0%
1%
2%
0%
1%
2%
WT
KI/KI

Figure 8

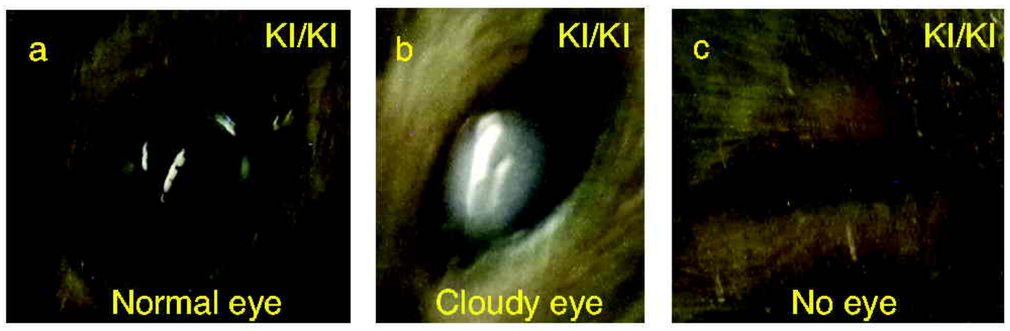

Mannose during pregnancy

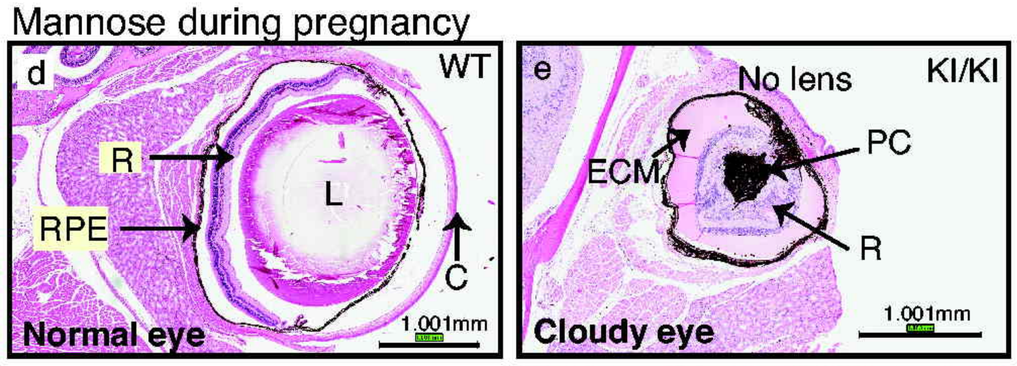

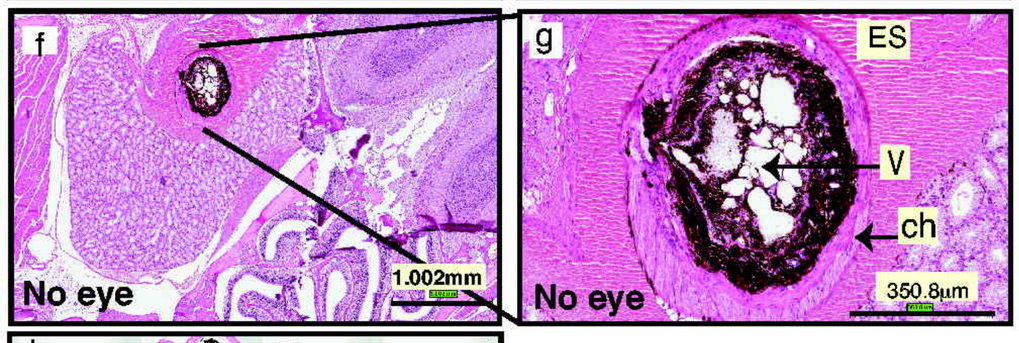

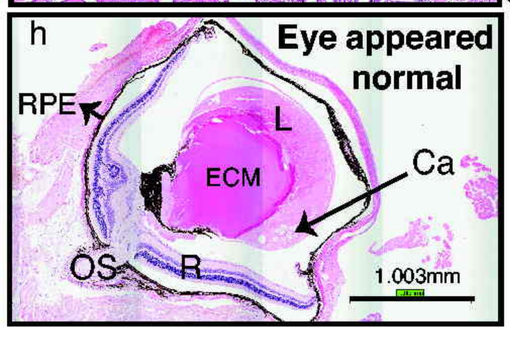

Mannose started at P1

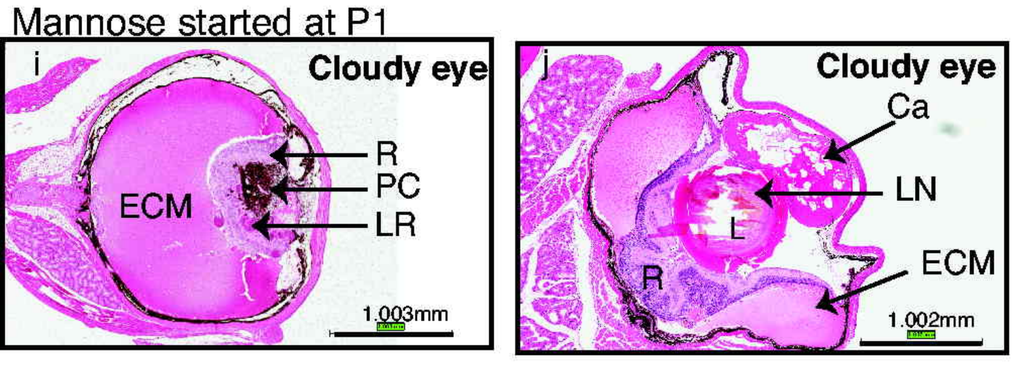

Figure.9

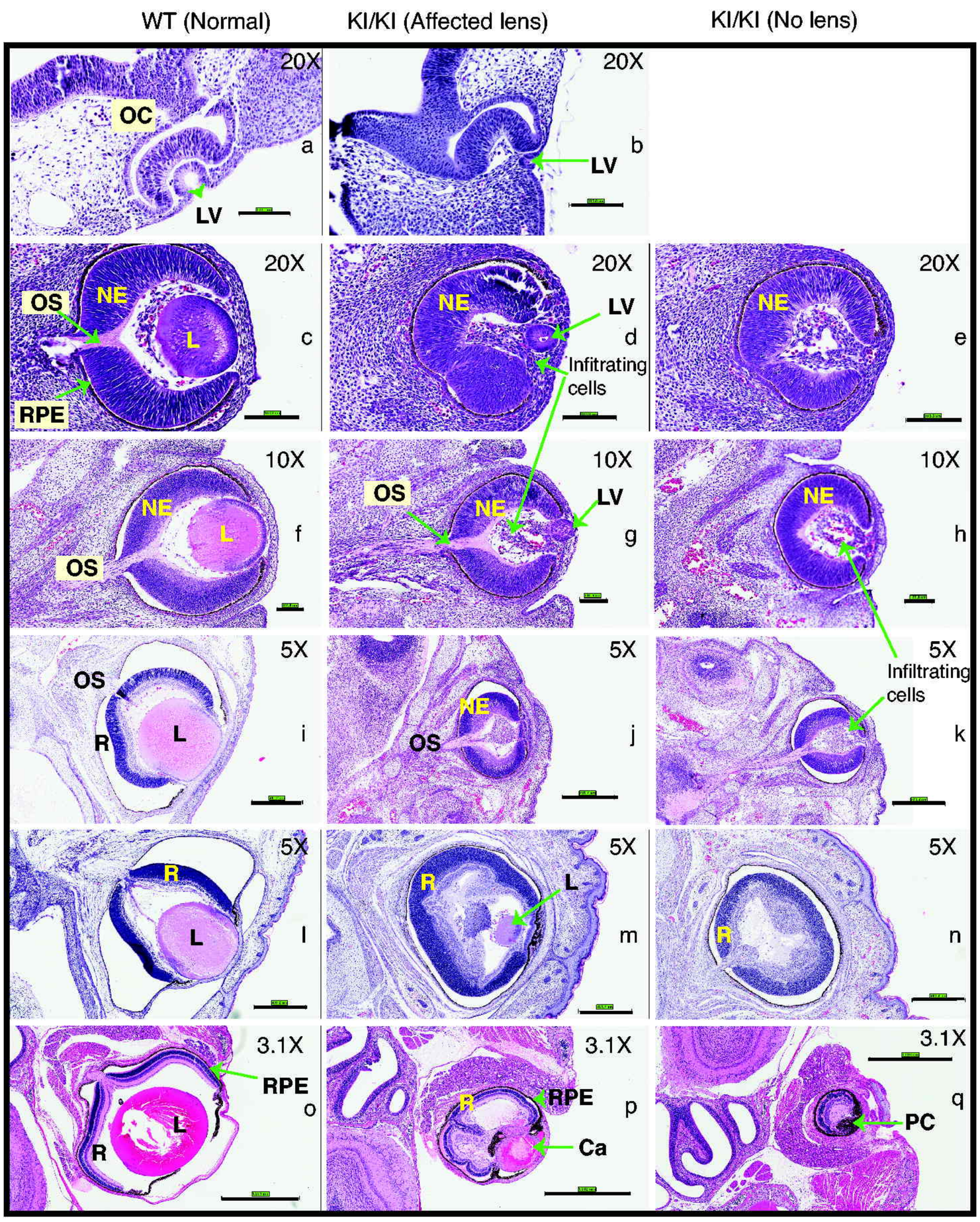
WT (Normal)
KI/KI (Affected lens)
KI/KI (No lens)
E10-11
E12-13
E14-15
E16-17
E18-19
P14
20X
OC
LV
a
b
OS
NE
L
RPE
c
Infitrating cells
d
e
10X
f
g
h
5X
R
i
j
Infiltrating cells
k
l
m
n
3.1X
o
p
Ca
q
PC

Figure. 10

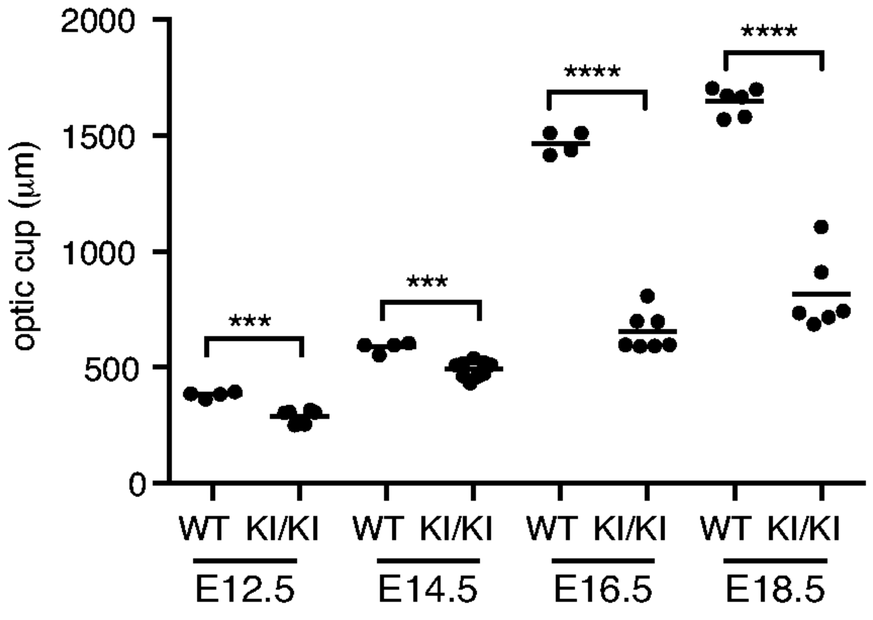
optic cup (μm)
2000
1500
1000
500
0
***
***
****
****
WT KI/KI WT KI/KI WT KI/KI WT KI/KI
E12.5
E14.5
E16.5
E18.5

Figure.11

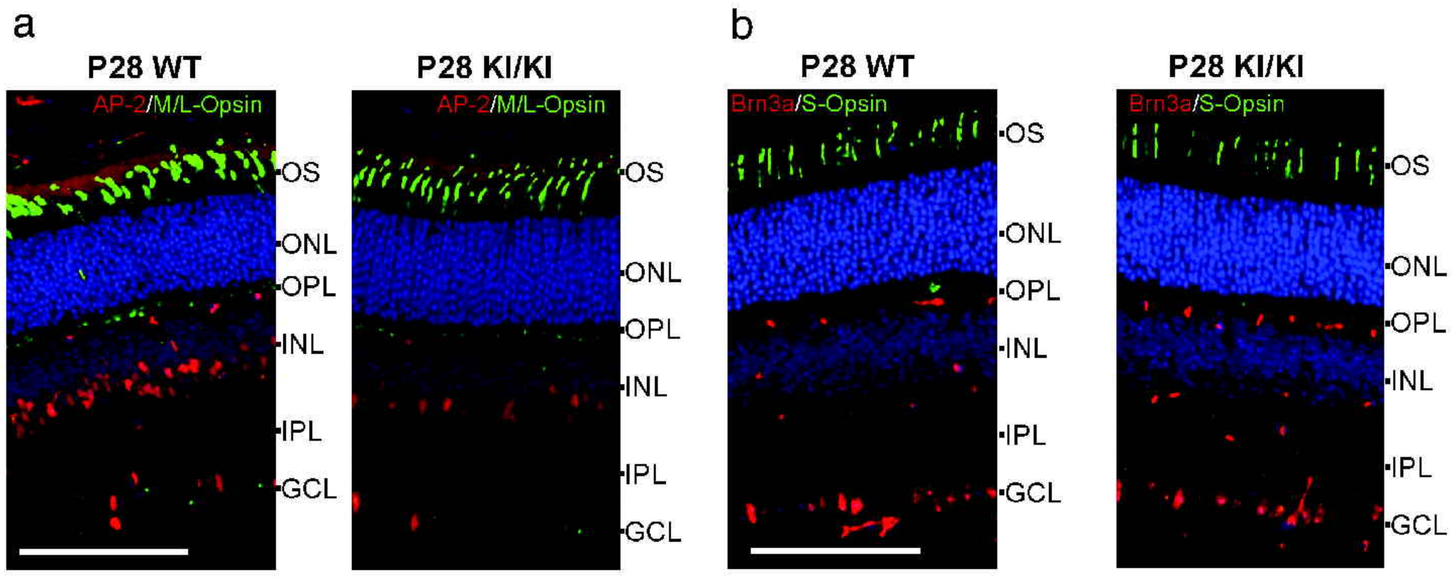
a
P28 WT
AP-2/M/L-Opsin
OS
ONL
OPL
INL
IPL
GCL
P28 KI/KI
AP-2/M/L-Opsin
OS
ONL
OPL
INL
IPL
GCL
b
P28 WT
Brn3a/S-Opsin
OS
ONL
OPL
INL
IPL
GCL
P28 KI/KI
Brn3a/S-Opsin
OS
ONL
OPL
INL
IPL
GCL

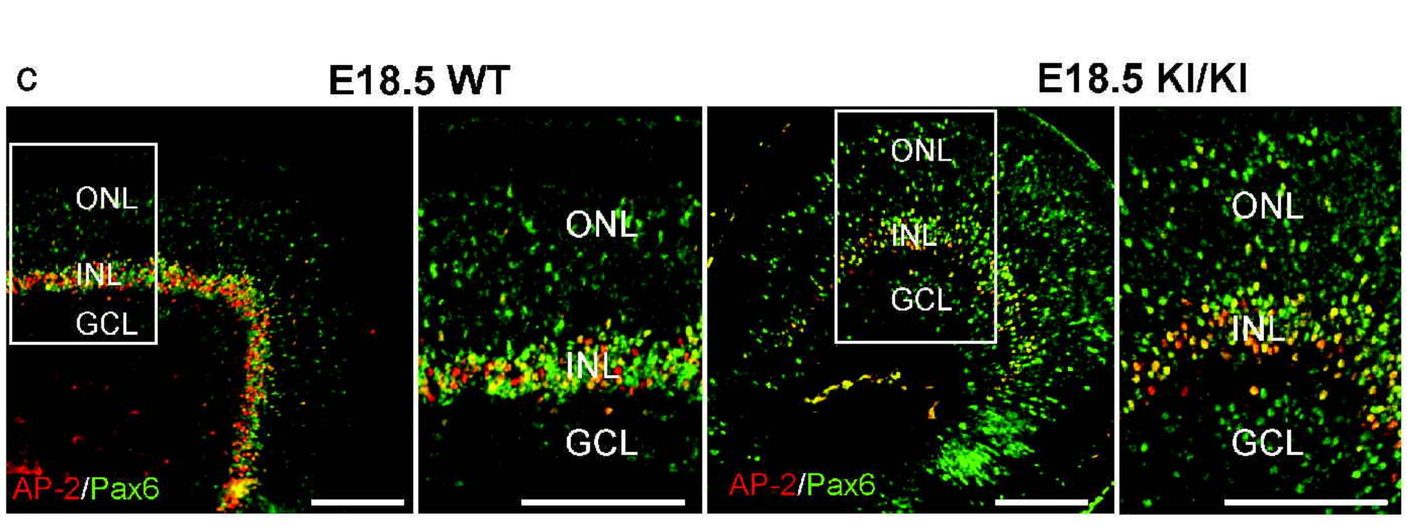
c
E18.5 WT
ONL
INL
GCL
AP-2/Pax6
ONL
INL
GCL
E18.5 KI/KI
ONL
INL
GCL
AP-2/Pax6
ONL
INL
GCL

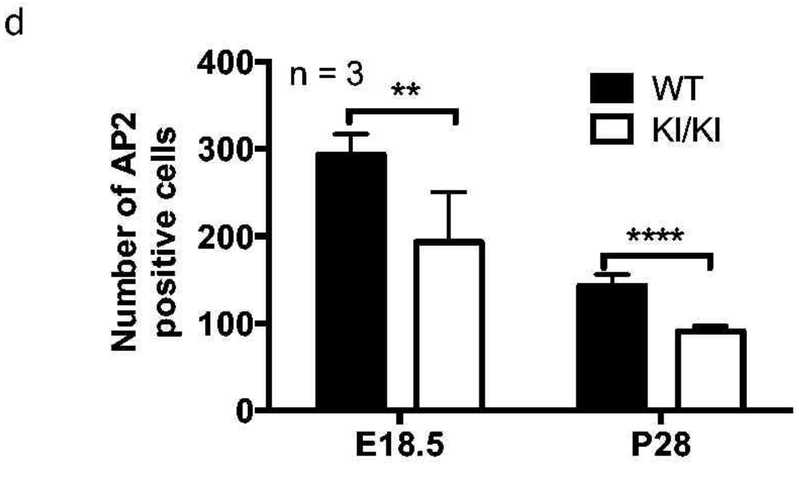
d
n = 3
**
****
WT
KI/KI
Number of AP2 positive cells
400
300
200
100
0
E18.5
P28

Figure.12

a

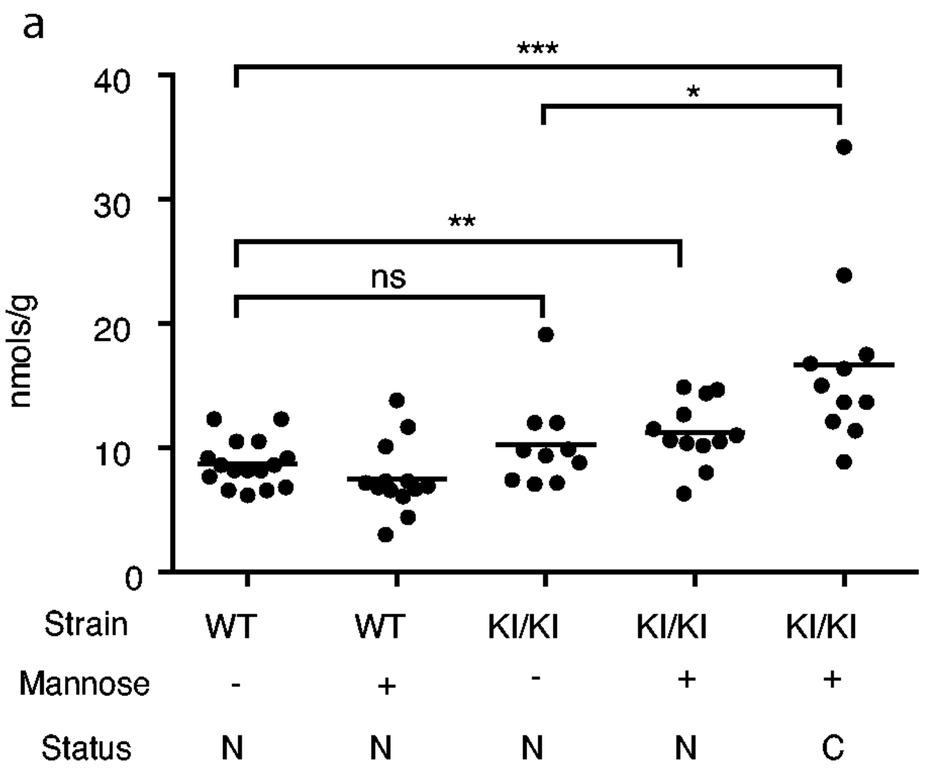
***
*
**
ns
40
30
20
10
0
nmols/g
Strain WT WT KI/KI KI/KI KI/KI
Mannose - + - + +
Status N N N N C

b

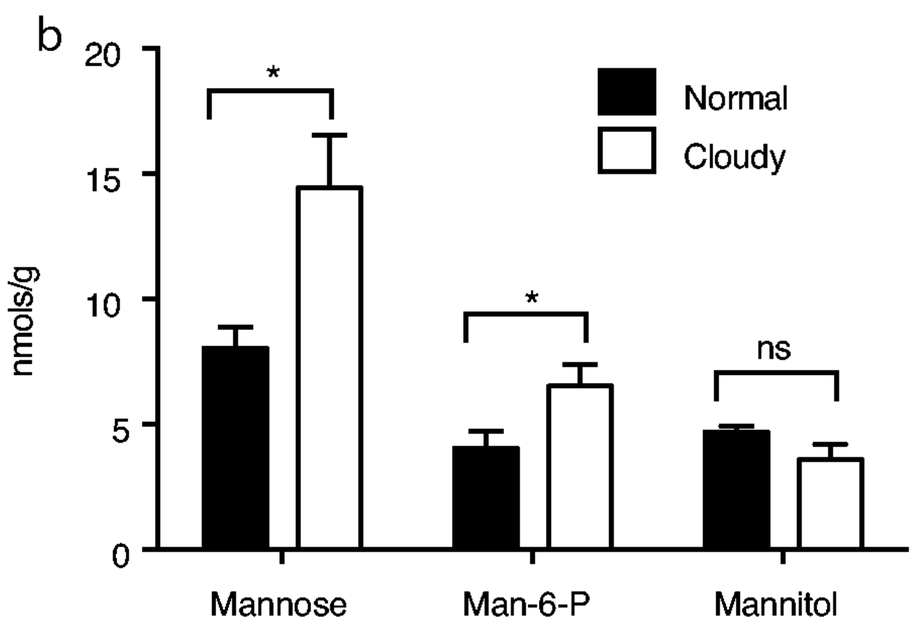
20
15
10
5
0
nmols/g
*
*
ns
Normal
Cloudy
Mannose
Man-6-P
Mannitol

SUPPLEMENTARY INFORMATION

Mpi Targeting and Generation of Mice: A 12kb clone containing exons 3-8 of mouse Mpi was isolated from a 129/SvJ lambda phage genomic library (formerly Stratagene, presently Agilent Technologies, Inc, Santa Clara, CA, USA). For generation of the Y255C substitution, site-directed mutagenesis introduced a mutation (ATCTAC => ATATGC) in the exon 6 coding sequence, which also introduced a new NdeI site for genotypic screening. A 1.9kb KpnI-SacII fragment from PM30 containing a PGK-neo selection cassette flanked by frt sites and a single loxP site was linked to HindIII sequences and cloned into the HindIII site between exons 4 and 5 (1). An additional loxP site was PCR amplified from pflox (2) and inserted into an EcoRI site distal to exon 8. Another BamHI site was engineered 5.6kb downstream of the distal loxP site to aid in Southern blot screening of targeted ES cells and mice. The final targeting construct in pBluescript (Agilent Technologies, Inc, Santa Clara, CA, USA) was linearized with NotI and electroporated into C57BL/6 embryonic stem (ES) cells.

Screening of targeted ES cells was done by Southern blot of BamHI digested genomic DNA (gDNA) using a 3' probe (31.6kb wt and 5.6kb targeted) or NheI digested gDNA using a 5' probe (14.0kb wt and 5.0kb targeted) (Supplement fig.1a and 1b). An 11.1kb band from SacI digested gDNA using a neo specific probe indicated the presence of the neo cassette (fig.1b). The mutation producing the Y255C change was confirmed by sequencing (data not shown). Chimera, F1 and F2 generation offspring were further confirmed by Southern blot, as described above (data not shown). The neo selection cassette was removed by crossing F2 generation mice to a germline FLP recombinase-expressing mouse line. M14a-F1 and LoxP-R1 primers were routinely used for PCR genotyping of the knock-in mice (Supplement fig.1c).

References

1. Meyers E.N., Lewandoski M., Martin G.R. (1998) An Fgf8 mutant allelic series generated by Cre- and Flp-mediated recombination. *Nat Genet*., 18(2):136–41.

2. Chui D., Oh-Eda M., Liao Y. F., Panneerselvam K., Lal A., Marek K. W., Freeze H. H., Moremen K. W., Fukuda M. N., Marth J. D (1997) Alpha-mannosidase-II deficiency results in dyserythropoiesis and unveils an alternate pathway in oligosaccharide biosynthesis. *Cell* 90, 157–67.

Supplement figure.1

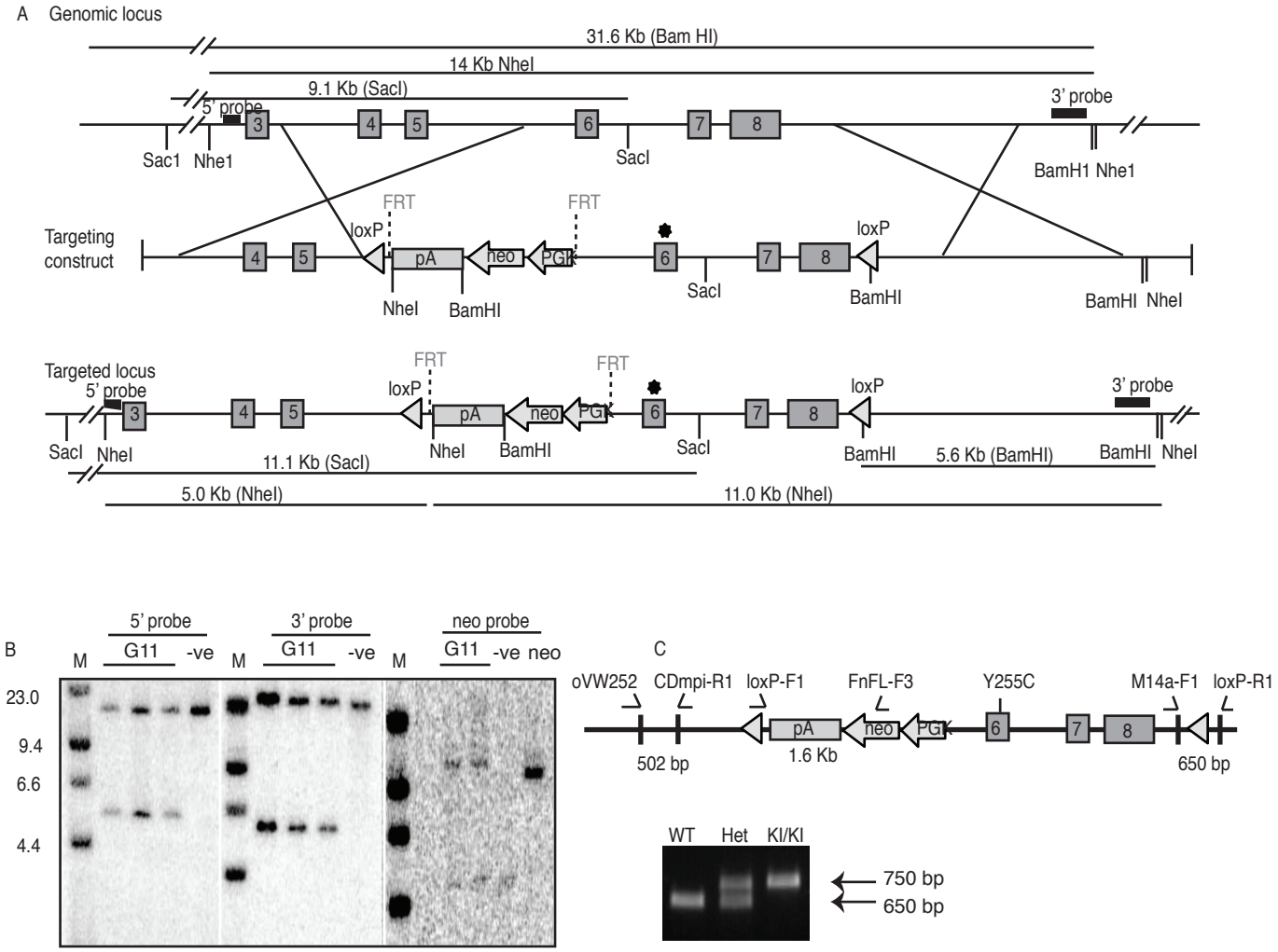

Gene targeting strategy and generation of MpiY255C mice. A) Schematic representation of exons 3 to 8 (gray numbered boxes) of the mouse WT Mpi genomic locus (top), design of targeting construct (middle) and resulting targeted genomic locus (bottom). The location of the Y255C coding mutation in exon 6 is indicated by an asterisk. Restriction sites used for Southern blot screening are indicated, as well as the associated WT and targeted fragment sizes. Locations of the 5'- and 3'-probes used for Southern screening are represented by black rectangles. The Neo probe is specific for the neo coding region. The neo selection cassette was flanked by FLP-recombinase recognition sites (FRT) and removed by crossing targeted animals with germline-expressing FLP mice. Although not used in this study, loxP sites (gray triangles) enclosing *Mpi* exons 6, 7 and 8 were engineered for CRE-mediated conditional knockout of *Mpi*. B) Southern blot analysis of targeted (G11) and WT (-ve) ES cell clones. Hybridization with the Neo probe also included a neo positive control (neo). Probes with the associated genomic digests are depicted in A and described in the text. C) Routine PCR genotyping of the distal loxP site with primers M14a-F1 and loxP-R1 was used to identify knock-in (KI/KI) animals in lieu of routine sequencing. A positive (loxP = Y255C) allele produces a 750 bp product while the wt allele produces a 650bp signal. Occasional direct sequencing of the Y255C locus from targeted pups was performed to confirm co-segregation of the Y255C mutation with the distal loxP-site, validating that loxP positive animals still possess the Y255C mutation. Key: neo, neomycin-resistance sequence; pA, poly(A) signal; PGK, phosphoglycerate kinase promoter; loxP, CRE- recombinase recognition sequence; FRT, FLP-recombinase recognition sequence.

Supplement figure.2.

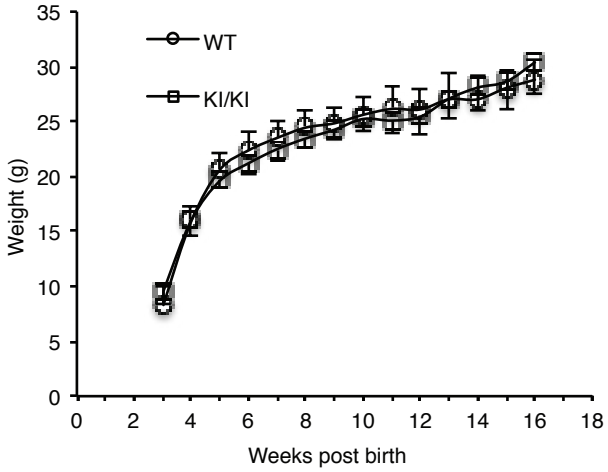

Body weights. Both KI and littermate WT mice were weighed weekly for 16 weeks starting at weaning (3 weeks).

Supplement figure.3

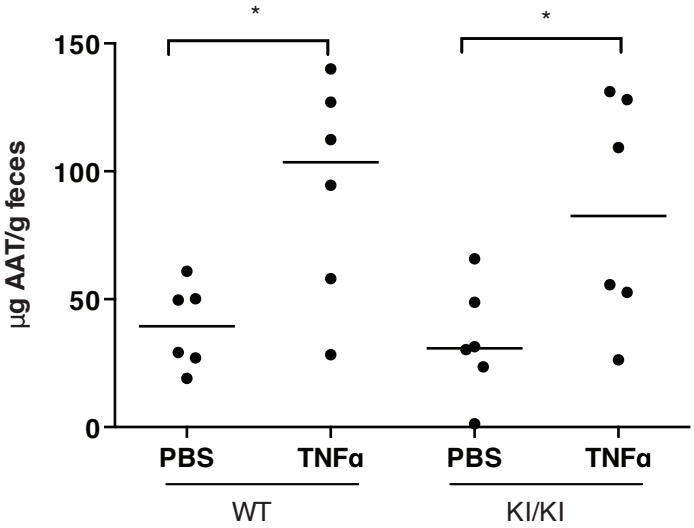

Enteric Protein Loss. Individually housed WT and KI/KI mice were injected with either PBS or 0.25 mg/kg TNFa. AAT in the fecal extracts was measured by ELISA. Each point represents data from an individual mouse. $p < 0.05$.

Supplement Table 1. Head rotations measured by motorized optic drum.

Genotype n = # of mice	Status of the Eyes	Clockwise rotation	Anticlockwise rotation
WT (n=8)	Normal eyes	8±3	7±3
KI/KI (n=8)	Normal eyes	10±2	8±2
KI/KI (n=12)	Right eye affected	0	9±3
KI/KI (n=3)	Left eye affected	8±3	0
KI/KI (n=11)	Both eyes affected	0	0